

# Global Biogeochemical Cycles®

## RESEARCH ARTICLE

10.1029/2025GB008526

### Key Points:

- Collapse of Atlantic Meridional Overturning Circulation increases North Atlantic preformed and regenerated Dissolved Inorganic Carbon (DIC)
- Decrease in Pacific DIC is dominated by regenerated DIC in a preindustrial simulation and by preformed DIC in a glacial simulation
- Novel decomposition of ocean carbon is accurate, whereas approximations of respired DIC based on Apparent Oxygen Utilization are unreliable

### Supporting Information:

Supporting Information may be found in the online version of this article.

### Correspondence to:

A. Schmittner,  
[andreas.schmittner@oregonstate.edu](mailto:andreas.schmittner@oregonstate.edu)

### Citation:

Schmittner, A., & Boling, M. (2025). Impact of Atlantic Meridional Overturning Circulation Collapse on Dissolved Inorganic Carbon components in the ocean. *Global Biogeochemical Cycles*, 39, e2025GB008526. <https://doi.org/10.1029/2025GB008526>

Received 30 JAN 2025

Accepted 31 OCT 2025

### Author Contributions:

**Conceptualization:** A. Schmittner  
**Data curation:** A. Schmittner  
**Formal analysis:** A. Schmittner  
**Funding acquisition:** A. Schmittner  
**Investigation:** A. Schmittner, M. Boling  
**Methodology:** A. Schmittner  
**Project administration:** A. Schmittner  
**Resources:** A. Schmittner  
**Software:** A. Schmittner  
**Supervision:** A. Schmittner  
**Validation:** A. Schmittner  
**Visualization:** A. Schmittner, M. Boling  
**Writing – original draft:** A. Schmittner  
**Writing – review & editing:**  
A. Schmittner

© 2025. American Geophysical Union. All Rights Reserved.

## Impact of Atlantic Meridional Overturning Circulation Collapse on Dissolved Inorganic Carbon Components in the Ocean

A. Schmittner<sup>1</sup>  and M. Boling<sup>2</sup> 

<sup>1</sup>College of Earth, Ocean, and Atmospheric Sciences, Oregon State University, Corvallis, OR, USA, <sup>2</sup>College of Physical Sciences and Engineering, Brigham Young University—Idaho, Rexburg, ID, USA

**Abstract** The Atlantic Meridional Overturning Circulation (AMOC) impacts temperatures, ecosystems, and the carbon cycle. However, AMOC effects on Earth's carbon cycle remains poorly understood, in part because contributions of different physical and biological mechanisms that impact carbon storage in the ocean are not typically diagnosed in climate models. Here, we explore modeled effects of AMOC shutdowns on ocean Dissolved Inorganic Carbon (DIC) by applying a new decomposition that explicitly calculates preformed and regenerated DIC components and separates physical and biological contributions. An extensive evaluation in transient simulations finds that the method is accurate, especially for basin-wide changes, whereas errors can be significant at global and local scales. In contrast, estimates of respiration carbon based on Apparent Oxygen Utilization lead to large errors and are generally not reliable. In response to a shutdown of the AMOC under Last Glacial Maximum (LGM) background climate, ocean carbon increases and then decreases, leading to opposite changes in atmospheric carbon dioxide ( $\text{CO}_2$ ). DIC changes are dominated by opposing changes in biological carbon storage. Whereas regenerated components increase in the Atlantic and dominate the initial increase in global ocean DIC until model year 1000, preformed components decrease in the other ocean basins and dominate the long-term DIC decrease until year 4000. Biological disequilibrium is an important contribution to preformed carbon changes. Biological saturation carbon decreases in the Pacific, Indian, and Southern Oceans due to a decrease in surface alkalinity. The spatial patterns of the DIC components and their changes in response to an AMOC collapse are presented.

## 1. Introduction

Large variations of the Atlantic Meridional Overturning Circulation (AMOC) have occurred in the past (Lynch-Stieglitz, 2017) and may be possible in the future (Bakker et al., 2016; Weijer et al., 2020). Millennial-scale AMOC variability during the last glacial cycle has been associated with aberrations in temperature (Buizert et al., 2024), atmospheric  $\text{CO}_2$  (Ahn et al., 2012; Wendt et al., 2024), and carbon cycling on land and in the ocean (Bauska et al., 2016, 2018; Menking et al., 2022). However, the mechanistic links between AMOC and the carbon cycle remain poorly understood.

A comparison of modeling studies designed to assess the effect of AMOC collapse on carbon cycling and atmospheric  $\text{CO}_2$  shows divergent results (Gottschalk et al., 2019). Although some models simulate an increase in atmospheric  $\text{CO}_2$  following a reduction in AMOC (Schmittner & Galbraith, 2008), others show a decrease (Menkveld et al., 2015). Moreover, even using the same model, an AMOC reduction can result in a different sign (Menkveld et al., 2008) or magnitude (Schmittner et al., 2007) of the atmospheric response depending on whether a glacial or modern background climate is used. Understanding these differences is complicated by the different physical and biological mechanisms that affect carbon storage in the ocean, which are not typically diagnosed in models. Here, we apply a new method to decompose Dissolved Inorganic Carbon  $\text{DIC} = \text{C}_{\text{pre}} + \text{C}_{\text{reg}}$  into preformed and regenerated components, while separating biological and physical contributions to better understand the simulated changes. The method has previously been applied to equilibrium simulations of the Last Glacial Maximum (LGM, ~20,000 years ago), demonstrating the accuracy of the decomposition and highlighting the importance of changes in biological disequilibrium components (Khatiwala et al., 2019). Here, we apply the method for the first time to transient simulations. We provide a comprehensive evaluation and illustrate changes in the temporal evolution and spatial patterns of the different components.

Approximations of regenerated components based on Apparent Oxygen Utilization (AOU) have been frequently used (Gruber et al., 1996; Menzel et al., 2017; Schmittner & Lund, 2015; Schmittner et al., 2013), but can have large errors (Duteil et al., 2013; Ito et al., 2004; Khatiwala et al., 2019). AOU would be a perfect estimator for respired carbon if dissolved oxygen was at equilibrium with the atmosphere everywhere at the surface ocean. However, at high latitudes oxygen is substantially undersaturated (Cliff et al., 2021; Russell & Dickson, 2003). The resulting oxygen disequilibrium propagates into the ocean interior, which compromises the use of AOU to estimate respired carbon. For example, Schmittner and Lund (2015) used AOU to estimate that an AMOC shutdown in a preindustrial climate would lead to a decrease in regenerated carbon by 400 Pg, dominating the total changes in ocean carbon and the resulting increase in atmospheric CO<sub>2</sub>. Here, we provide an additional assessment of those approximations by comparing them with the precise components calculated in transient simulations.

Recent studies have questioned the idea that the AMOC collapsed completely during Heinrich Stadial 1 (HS1) (Oppo et al., 2015; Pöppelmeier et al., 2023; Repschläger et al., 2021). Thus, our simulations presented here, which explore the effect of a complete AMOC collapse, are idealized and are not meant to reproduce changes during HS1 or any other specific paleo event.

This paper presents a detailed description of the carbon cycle results. The results on carbon isotopes will be reported in a companion paper (Schmittner, 2025a).

## 2. Methods

### 2.1. Model Description

The Oregon State University version of the University of Victoria climate model (OSU-U Vic) version 2.9.10 is used as in Schmittner and Fillman (2024). Its three-dimensional ocean component is coupled with a computationally efficient atmospheric energy moisture balance model, a land surface and vegetation module, a dynamic-thermodynamic sea ice component, and the process-based Model of Ocean Biogeochemistry and Isotopes (MOBI), all run at a coarse resolution of 1.8 × 3.6°. MOBI includes four plankton functional types (diatoms, diazotrophs, other phytoplankton and zooplankton), nutrients (nitrate, phosphate, silicate and iron), semi-refractory dissolved organic carbon (Somes & Oschlies, 2015), and variable stoichiometry (Fillman et al., 2023). C and <sup>13</sup>C are tracked in the ocean, land, and atmospheric components. Note that the model version used here does not include interactive sediments and permafrost. Thus, a closed system approach is taken with regard to C and <sup>13</sup>C, which are conserved in the land-atmosphere-ocean system. This approximation should be valid for millennial timescales, which will be the focus of this paper, since sediment interactions are believed to play a role only on timescales longer than about 5000 years (Archer et al., 1998).

The atmospheric component uses prescribed seasonally varying winds and atmospheric co-albedo (Weaver et al., 2001), rather than interactive winds and clouds. This is a caveat, as changes in AMOC are expected to affect winds and clouds, which could modulate C and <sup>13</sup>C on land and in the surface ocean (Buzert et al., 2018; Chiang & Bitz, 2005; Frierson et al., 2013), although a previous study indicates that wind-driven changes are relatively small (Schmittner & Lund, 2015). The advantage of using such a simple atmospheric component is that the model is computationally efficient, which allows multiple millennial scale simulations and sensitivity tests. Changes in winds are considered in our LGM simulations, by applying anomalies from models with dynamic atmospheres (Muglia & Schmittner, 2015), but those anomalies are not changing as the AMOC changes in the experiments presented here. Model results have been extensively validated against present day observations and reconstructions from the LGM. Here we mainly use as initial conditions an equilibrated data-constrained LGM version (Khatiwala et al., 2019; Muglia et al., 2017; Schmittner & Fillman, 2024). Thus, most of the simulations described here represent glacial climates of the Pleistocene, although some results from preindustrial runs are also included for comparison.

### 2.2. Carbon Decomposition

For the decomposition of DIC, we explicitly track  $C_{pre}$ ,  $C_{sat}$ ,  $C_{soft}$ ,  $C_{caco_3}$  (Table 1). Regenerated components ( $C_{reg} = C_{soft} + C_{caco_3}$ ) from the remineralization of soft tissue organic matter ( $C_{soft}$ ) and dissolution of calcium carbonate ( $C_{caco_3}$ ) are calculated directly by accumulating the DIC sources of the model in the interior, while setting surface concentrations to zero. Preformed and saturation components,  $C_{pre}$  and  $C_{sat}$ , are equal to the

**Table 1**  
*Components of DIC*

Abbreviation	Calculation	Description
DIC	DC ( <i>Full</i> )	Total Dissolved Inorganic Carbon
$C_{pre}$	DC ( <i>Full</i> )	Preformed Carbon
$C_{sat}$	DC ( <i>Full</i> )	Saturation Carbon
$C_{dis}$	$C_{pre} - C_{sat}$	Disequilibrium Carbon
$C_{pre,phy} = C_{phy}$	DC ( <i>NoBio</i> )	Physical (Preformed) Carbon
$C_{sat,phy}$	DC ( <i>NoBio</i> )	Physical Saturation Carbon
$C_{dis,phy}$	$C_{pre,phy} - C_{sat,phy}$	Physical Disequilibrium Carbon
$C_{pre,bio}$	$C_{pre} - C_{pre,phy}$	Biological Preformed Carbon
$C_{sat,bio}$	$C_{sat} - C_{sat,phy}$	Biological Saturation Carbon
$C_{dis,bio}$	$C_{dis} - C_{dis,phy} = C_{pre,bio} - C_{sat,bio}$	Biological Disequilibrium Carbon
$C_{soft}$	DC ( <i>Full</i> )	Soft-Tissue Carbon
$C_{caco3}$	DC ( <i>Full</i> )	Calcium Carbonate Carbon
$C_{reg}$	$C_{soft} + C_{caco3}$	Regenerated Carbon
$C_{bio}$	$C_{reg} + C_{pre,bio}$	Biological Carbon
$\Sigma$	$C_{pre} + C_{reg} = C_{phy} + C_{bio}$	Sum of Components
$\epsilon$	$\Sigma - \text{DIC}$	Error of Decomposition

*Note.* Directly calculated (DC) components are indicated in the second column with the model in brackets. Total components are calculated using the *Full* model, which includes both physics and biology. Physical components are calculated using model *NoBio*, which excludes biology. Formulas are provided for other components. Since model *NoBio* has no regenerated components physical carbon is only preformed.

surface concentrations of DIC and  $\text{DIC}_{sat}$ , respectively, and then propagated into the interior without subsurface sources or sinks. The saturation component represents the DIC concentration surface water would have if it was at equilibrium with the atmosphere. Disequilibrium components,  $C_{dis} = C_{pre} - C_{sat}$ , are the differences between preformed and saturation components.

In addition to the main experiment, which is referred to as *LGM Full* in the following, we have constructed two other models. Ocean biology has been removed in model *LGM NoBio* and fluxes between the atmosphere and the land in the calculation of atmospheric  $\text{CO}_2$  and  $\delta^{13}\text{C}_{\text{CO}_2}$  have been set to zero in model *LGM NoLand*. Thus, model *LGM NoLand* represents an ocean-atmosphere-only carbon cycle, which is useful, compared to model *LGM Full*, in quantifying contributions to atmospheric  $\text{CO}_2$  changes from land carbon variations. Model *LGM NoBio* represents a physics-only ocean carbon cycle and yields the physical components of the decomposition, for example,  $C_{dis,phy}$ . Biological components are diagnosed as the difference from the *LGM Full* model, for example,  $C_{dis,bio} = C_{dis} - C_{dis,phy}$ . The biological disequilibrium component arises, for example, from upwelling of respired carbon, which leads to oversaturation. If the resulting outgassing is incomplete, as it is the case in the Southern Ocean, then the water returning to the subsurface will have an excess of carbon. Thus,  $C_{dis,bio}$  is positive almost everywhere in the ocean. The physical disequilibrium arises, for example, from upwelling of relatively warm waters in the Antarctic divergence and cooling of that water as it moves south. This increases the solubility of DIC and leads to undersaturation and ingassing. Since that ingassing is incomplete the waters that subduct back into the interior as AABW have a DIC deficit. Thus,  $C_{dis,phy}$  is negative in AABW. The biological saturation component  $C_{sat,bio}$  is due to the effect of biology on alkalinity. Calcium carbonate production decreases surface alkalinity, which decreases saturation DIC and leads to negative values for  $C_{sat,bio}$ . In contrast, temperature and salinity affect  $C_{sat,phy}$ . Cooler temperatures, for example, increase the solubility of carbon in sea water and hence  $C_{sat,phy}$ . More details on the different components and how they change in LGM simulations can be found in Khatiwala et al. (2019) and Schmittner and Fillman (2024).

Thus, the full decomposition for DIC is

$$\text{DIC} = C_{\text{soft}} + C_{\text{caco}_3} + C_{\text{sat,phy}} + C_{\text{sat,bio}} + C_{\text{dis,phy}} + C_{\text{dis,bio}} - \epsilon, \quad (1)$$

where  $\epsilon$  represents the error of the decomposition. Since preformed and regenerated components are calculated independently, their sum  $\Sigma = C_{\text{reg}} + C_{\text{pre}}$  is not necessarily equal to the independently simulated DIC concentration. This allows us to evaluate the method by quantifying the error as  $\epsilon = \Sigma - \text{DIC}$ . We also use a model with preindustrial background climate, referred to as *PI Full*, the results of which are illustrated in Supporting Information S1.

### 2.3. Model Spin-Up and Experimental Design

The models are spun up in stages as in Schmittner and Fillman (2024). Following a 7000-year phase with prescribed  $\text{CO}_2 = 280$  ppm and other forcings under preindustrial conditions,  $\text{CO}_2$  is allowed to vary according to land-atmosphere and ocean-atmosphere carbon fluxes. Once equilibrated, LGM boundary conditions (ice sheets, aeolian soluble iron fluxes, sea level effects on sedimentary iron and nitrogen fluxes, radiative effects of methane and nitrous oxide, whole ocean increase in salinity, wind stress anomalies, changes in southern hemisphere moisture diffusivities; Muglia et al., 2018) are imposed instantaneously, leading to a decrease in  $\text{CO}_2$  to about 190 ppm, cooling of global temperatures, increased sea ice cover, and a shallower and weaker ( $\sim 11$  Sv) AMOC compared to the preindustrial simulation, consistent with other work (Gebbie, 2014; Men viel et al., 2017; Pöppelmeier et al., 2023). More information about the modeled LGM state is available elsewhere (Khatiwala et al., 2019; Schmittner & Fillman, 2024). Model *LGM NoBio* was equilibrated with an atmospheric  $\text{CO}_2$  concentration of 190 ppm for 6 ka, followed by a 1000-year phase with prognostic  $\text{CO}_2$ , leading to an almost identical climate as the model *LGM Full*. Cooling of global surface air temperatures in both models is  $5.7^\circ\text{C}$ , comparable with two recent observation-based estimates ( $-6.1 \pm 0.2^\circ\text{C}$  and  $-4.5 \pm 0.9^\circ\text{C}$ ) (Annan et al., 2022; Tierney et al., 2020).

The freshwater hosing experiments conducted here to perturb the AMOC are similar to previous work. Results regarding physics, the carbon cycle, and  $\delta^{13}\text{C}$  are comparable to Schmittner et al. (2007) and Schmittner and Lund (2015) and will not be discussed in detail here. We apply a freshwater flux into the North Atlantic that linearly increases from zero at (arbitrary) model year 0 to 0.3 Sv at model year 500 after which it is set to zero (Figure 1).

## 3. Response of AMOC, $\text{CO}_2$ and Carbon Inventories

As expected, the AMOC, in both the *LGM Full* model and in *LGM NoBio*, collapses in response to the forcing within the first  $\sim 300$  years and stays in the shut-down state for the remainder of the 4000-year long simulations (Figures 1 and 2).  $\text{CO}_2$  decreases in the *LGM Full* model during the first 500 years by 4–5 ppm and increases slowly thereafter by about 8–9 ppm until year 4000. However, approaching the AMOC-off equilibrium,  $\text{CO}_2$  is only 4 ppm higher than in the AMOC-on equilibrium at year 0. The  $\text{CO}_2$  variations in model *LGM Full* are almost entirely due to changes in biological ocean carbon storage as illustrated by model *LGM NoBio*, which shows only minor changes in  $\text{CO}_2$  of less than 2 ppm. In contrast, model *LGM NoLand* shows larger changes (11–12 ppm) than *LGM Full*, indicating that terrestrial carbon buffers atmospheric  $\text{CO}_2$  changes in *LGM Full*. This is due to carbon fertilization of terrestrial photosynthesis, which leads to enhanced land carbon storage at higher  $\text{CO}_2$  (Chen et al., 2022).

The initial decrease in atmospheric  $\text{CO}_2$  in model *LGM Full* is due to an increase in ocean carbon by about 30 Pg, whereas land carbon changes little over the first 300 years, but decreases rapidly afterward by up to 20 Pg around year 700 (Figure 1c). Physical processes only lead to much smaller changes in ocean carbon in model *LGM NoBio*, confirming the dominating role of ocean biology in the response of the model *LGM Full*. Changes in ocean carbon in *LGM NoLand* are muted compared to the *LGM Full* model, probably due to the larger atmospheric carbon response. For example, lower  $\text{CO}_2$  in *LGM NoLand* between years 500 and 1500 would lead to more outgassing from the ocean and thus lower ocean carbon.

Comparison with model *LGM NoBio*, which has a much smaller land carbon response, suggests that carbon fertilization dominates the land carbon evolution in model *LGM Full*. In fact, land carbon increases in *LGM NoBio*

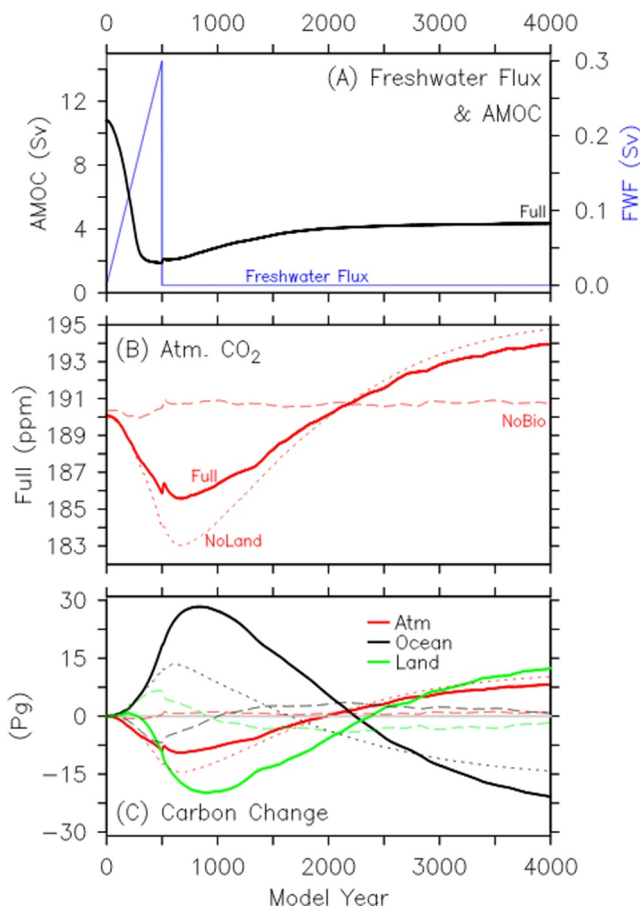


**Figure 1.** Timeseries of forcing and response in model *LGM Full*. (a) Freshwater forcing (blue line, right axis) and AMOC (left axis) in models *LGM Full* (black solid line). AMOC in *LGM NoBio* is indistinguishable from *LGM Full*. (b) Atmospheric CO<sub>2</sub> in models *LGM Full* (red solid, left axis), *LGM NoBio* (red dashed, right axis) and *LGM NoLand* (red dotted, left axis). (c) Change in Carbon Inventories in the Atmosphere (red), ocean (black) and land (green) in models *LGM Full* (solid), *LGM NoBio* (dashed) and *LGM NoLand* (dotted).

decrease is dominated by saturation carbon changes, which peaks slightly earlier around year 1400. Physical changes ( $C_{sat,phy}$ ) contribute about 30 Pg, but biology ( $C_{sat,bio}$ ) dominates by contributing about 110 Pg. Subsequently, however, biological saturation carbon increases again, such that in year 4000 it is only ~10 Pg lower than in year 0, whereas the biological disequilibrium decrease between years 1000 and 4000 compensates for most of the  $C_{sat,bio}$  changes, resulting in only a slight increase in preformed carbon during the second half of the simulation. Biological saturation carbon changes are dominated by the effect of biology on alkalinity as will be discussed in more detail in Section 4.2.2. Biological production of calcium carbonate removes alkalinity from surface waters and thus reduces the saturation concentration of DIC.

The AOU approximation overestimates  $C_{soft}$  in year 0 by 1,420 Pg consistent with earlier work (Schmittner & Fillman, 2024). However, it accurately reproduces the simulated changes of  $C_{soft}$  until about year 700. After that, it results in a much larger decrease than  $C_{soft}$ , such that at the end of the simulation  $C_{soft,AOU}$  has decreased about 80 Pg more than  $C_{soft}$ , resulting in a wrong sign of the changes with respect to year 0. The AOU approximation appears to include some of the biological disequilibrium changes of ~100 Pg, but  $C_{soft,AOU}$  underestimates  $C_{soft} + C_{dis,bio}$ , as may be expected considering that carbon has a longer equilibration time with respect to the atmosphere than oxygen (~1 year vs. ~1 month). However, the changes in  $C_{soft,AOU}$  approximate  $C_{soft} + C_{dis,bio}$  better than  $C_{soft}$ .

during the first 500 years, suggesting that climate changes associated with the shut-down of AMOC in the model favor the growth of terrestrial carbon. In model *LGM NoBio* both Net Primary Production (NPP) and soil respiration decrease over the first 500 years (not shown), but the decrease in soil respiration due to cooling around the North Atlantic is larger than the decrease in NPP, which leads to a net growth of terrestrial carbon.

## 4. Carbon Decomposition

### 4.1. Temporal Global and Basin-Wide Changes

Changes in the simulated carbon inventory in the whole ocean are almost fully determined by DIC, while the changes of Dissolved Organic Carbon (DOC) are negligible (Figure 3). The model's DOC inventory is much smaller than that of DIC and increases from 45 to 49 PgC due to the AMOC shutdown. However, recall that the model includes only semi-refractory DOC and does not include refractory DOC; thus, a considerable DOC component is missing in the model.

In year zero, the sum of the DIC components  $\Sigma = C_{pre} + C_{reg}$  overestimates the true DIC content of the ocean by 0.4% or 138 Pg (Schmittner & Fillman, 2024). This difference is removed from  $\Sigma$  in Figure 3a to better compare the AMOC-induced changes with those of DIC. The whole ocean change in  $\Sigma$  is very similar to that of DIC (Figure 3), both showing initial increases until about the year 1000 followed by slow declines thereafter. However, the increase in  $\Sigma$  is larger than that of DIC, indicating imperfections in the decomposition, especially on the global scale. The error of the decomposition  $\epsilon = \Sigma - \text{DIC}$  increases by 16 Pg to reach 154 Pg in the year 1500, after which it decreases again to 141 Pg at year 4000.

The decomposition reveals that the global ocean changes in DIC are relatively small residuals of large opposing changes in preformed and regenerated components (Figure 3). Whereas regenerated carbon increases, preformed carbon decreases. The initial increase in global DIC until about year 1000 is dominated by a large and rapid increase in respired soft-tissue carbon by about 100 Pg, which peaks around year 1300. DIC from calcium carbonate dissolution increases by ~70 Pg and slower, reaching a peak about 500 years later. Increases in  $C_{reg}$  are largely, but not fully, compensated for by a decrease in preformed carbon of ~140 Pg, peaking around year 1800. This

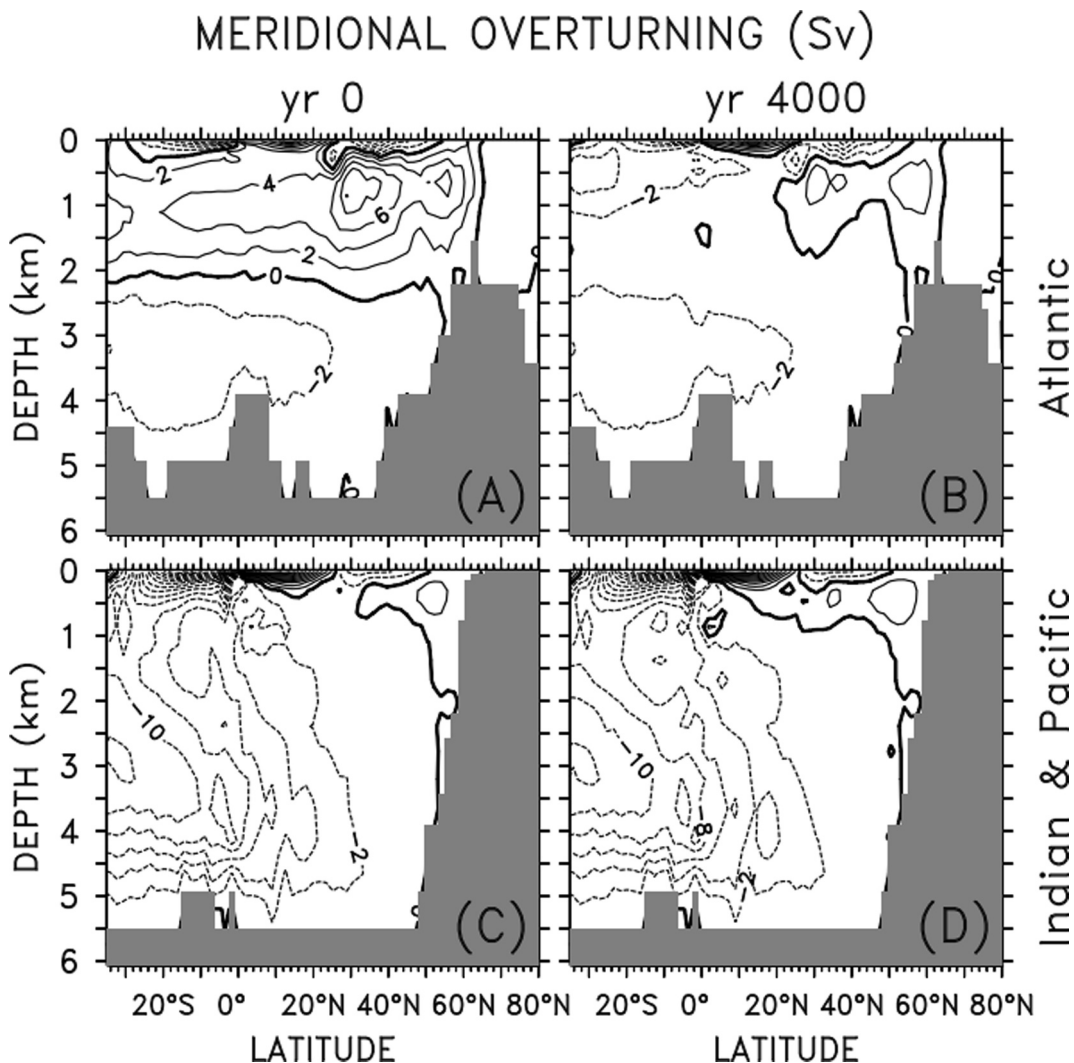


**Figure 2.** Meridional overturning streamfunction in Sv ( $1 \text{ Sv} = 10^6 \text{ m}^3 \text{ s}^{-1}$ ) in Atlantic (a, b) and Indian/Pacific (c, d) oceans at model years 0 (a, c) and 4000 (b, d) as a function of latitude and depth.

As in Schmittner et al. (2007), the relatively small changes in the DIC of the whole ocean are the net result of much larger redistributions of carbon between the ocean basins (Figures 4 and 5). DIC in the Atlantic rapidly increases by 227 Pg until year 1,000, peaks around year 1,500 at 7,466 Pg, and subsequently declines slightly by 12 Pg until year 4,000. In contrast, Pacific, Indian, and Southern Ocean DIC decreases by about 210 Pg by year 1,000, after which it slowly declines by an additional 47 Pg until year 4,000. This redistribution is a consequence of reducing the large differences in DIC between the Atlantic and Pacific in the AMOC-on configuration as will be discussed in more detail below in Section 4.2.

The decomposition is much more accurate for the basin-wide changes than for the whole-ocean changes. The sum of the components follows DIC very closely in all ocean basins. In the Atlantic,  $\Sigma$  overestimates the changes in DIC by up to 9 Pg at year 1,500, which corresponds to 3.8% of the DIC changes from year 0. Similarly for the Pacific, Indian and Southern Oceans,  $\Sigma$  underestimates changes by up to 7 Pg around year 1,600, or 2.8% of the DIC changes since year 0.

In contrast, the AOU approximation overestimates changes of  $C_{soft}$  in the Atlantic by up to 51 Pg in year 800, which corresponds to 62% of the changes from year 0, although the shapes of the curves are similar. In the Pacific, Indian and Southern Oceans  $C_{soft}$  does not change much, while  $C_{soft,AOU}$  decreases substantially. Again,  $C_{soft,AOU}$  seems to fall within  $C_{soft}$  and  $C_{soft} + C_{dis,bio}$ , in all basins, while approximating  $C_{soft} + C_{dis,bio}$  better than  $C_{soft}$ .

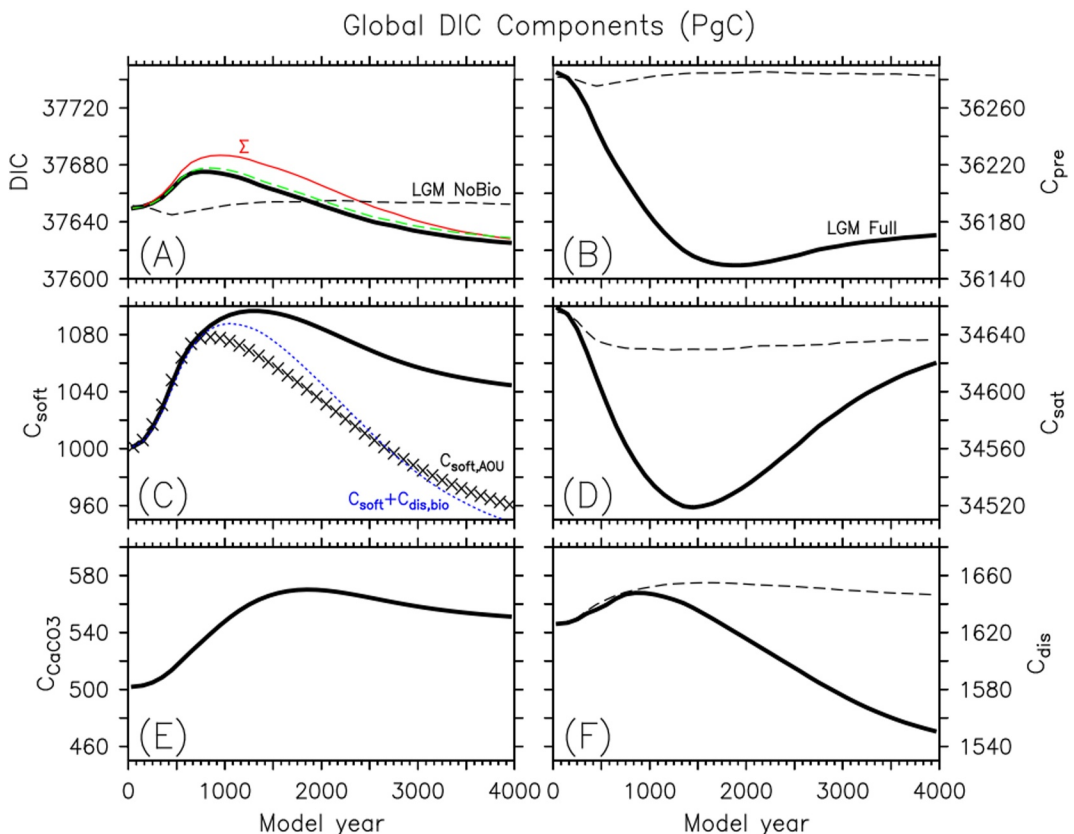


**Figure 3.** Global DIC components in PgC in models *LGM Full* (thick solid black) and *LGM NoBio* (dashed black). The range of the vertical axis is 150 Pg in all panels. (a) DIC. The thin green dashed line shows the change ( $C_{ocn} - \text{DOC}(t = 0)$ ) in the total ocean carbon inventory  $C_{ocn} = \text{DIC} + \text{DOC}$  adjusted for its difference with the DIC inventory at  $t = 0$  ( $\text{DOC}(t = 0) = 45$  Pg). The red thin line shows the change  $\Sigma(t) - \Sigma(t = 0) + \text{DIC}(t = 0)$  in the sum of the components  $\Sigma = C_{pre} + C_{reg}$  adjusted for its difference with DIC at  $t = 0$  ( $\Sigma(t = 0) = 37,788$  Pg). (b) Preformed carbon  $C_{pre}$  (solid) and  $C_{pre,phy}$  (dashed). (c) Soft-tissue remineralized carbon  $C_{soft}$ . Symbols show results from the AOU approximation adjusted by its difference  $C_{soft,AOU}(t = 0) - C_{soft}(t = 0) = 1,400$  Pg with  $C_{soft}$  at year 0. The blue dashed line shows modeled  $C_{soft} + C_{dis,bio}$ . (d) Saturation carbon  $C_{sat}$  (solid) and  $C_{sat,phy}$  (dashed). (e) Carbon from dissolved calcium carbonate  $C_{caco_3}$ . (f) Disequilibrium carbon  $C_{dis}$  (solid) and  $C_{dis,phy}$  (dashed). Results from *LGM NoBio* have been adjusted for the differences with *LGM Full* at year 0. For reference,  $\text{DIC}_{LGMNoBio}(t = 0) = C_{phy}(t = 0) = C_{pre,phy}(t = 0) = 35,221$  Pg,  $C_{sat,NoBio}(t = 0) = C_{sat,phy}(t = 0) = 35,968$  Pg,  $C_{dis,NoBio}(t = 0) = C_{dis,phy}(t = 0) = -747$  Pg.

Whereas  $C_{soft}$  does not change much in the Pacific, Indian and Southern Oceans, in the Atlantic it increases by 91 Pg until year 1,000, peaks around year 1500 and slowly decreases afterward. This increase is due to decreased ventilation, which allows respired carbon to accumulate. In the Atlantic, changes in  $C_{soft}$  are only surpassed by  $C_{pre}$ , which increases by 109 Pg until year 1000 and slowly increases by another 10 Pg until year 4000. As will be shown in more detail below, this increase in preformed carbon is due to reduced downward advection of relatively low preformed carbon from the surface. Thus, in the Atlantic,  $C_{pre}$  and  $C_{soft}$  changes are similar and conspire to enhance carbon storage. The initial increase in  $C_{pre}$  in the Atlantic is dominated by  $C_{dis,bio}$ , while  $C_{sat,bio}$  contributes to the stabilization in  $C_{pre}$  after year 1000 despite a decrease in  $C_{dis}$ . In contrast, in the Pacific the initial decrease in  $C_{pre}$  is dominated by  $C_{sat,bio}$ , which peaks around year 1500, while a slower decreasing trend in  $C_{dis,bio}$  leads to  $C_{dis,bio}$  being the dominant component toward year 4000.

#### 4.2. Spatial Distributions

Horizontally averaged DIC concentrations increase from about 1.95 mol/m<sup>3</sup> at the surface to around 2.4 mol/m<sup>3</sup> at depths below about 3 km in all ocean basins (Figure 6). Most of that vertical gradient of ~0.45 mol/m<sup>3</sup> is due to preformed carbon (~0.4 mol/m<sup>3</sup>) and saturation carbon contributes about half of the gradient. However, in the

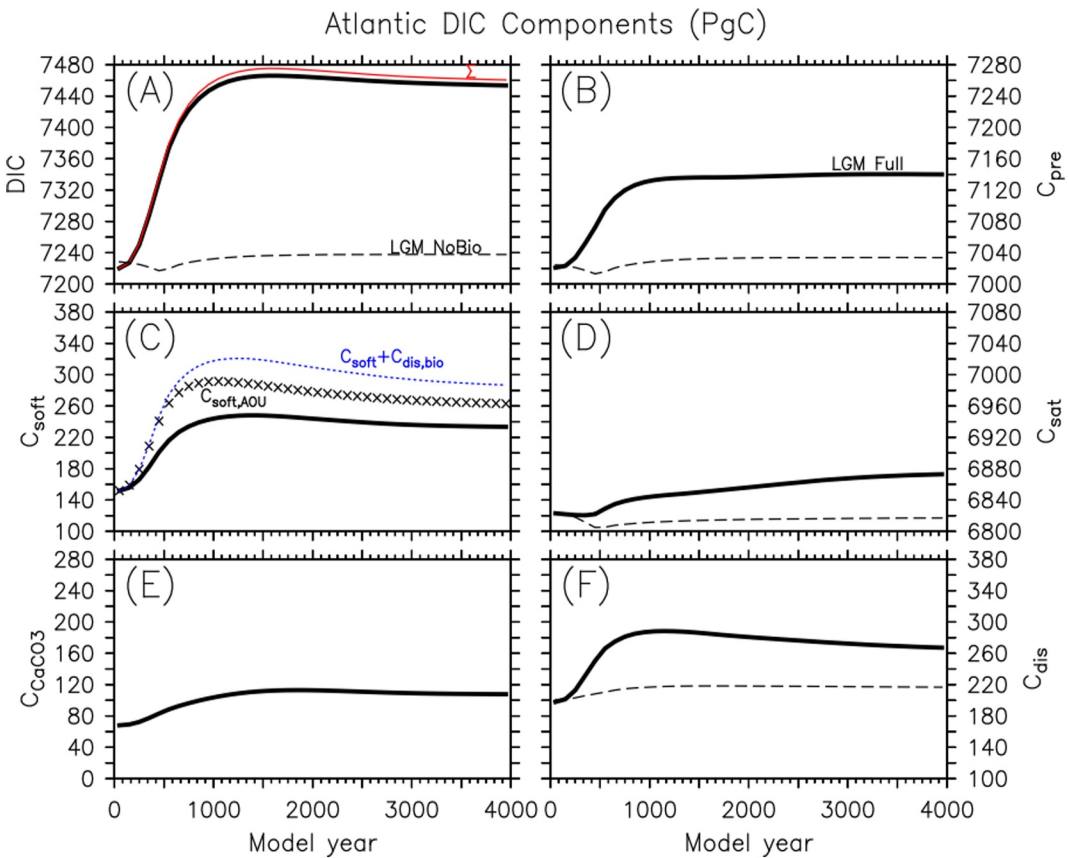


**Figure 4.** As Figure 3 but for Atlantic north of 40°S. The range of the vertical axis is 280 Pg in all panels.  $\Sigma(t = 0) = 7,241 \text{ Pg}$ ,  $C_{phy}(t = 0) = C_{pre,phy}(t = 0) = 6,993 \text{ Pg}$ ,  $C_{soft,AOU}(t = 0) = 345 \text{ Pg}$ ,  $C_{sat,phy}(t = 0) = 7,148 \text{ Pg}$ ,  $C_{dis,phy}(t = 0) = -158 \text{ Pg}$ .

case of an active AMOC (year 0, solid lines in Figures 6a and 6c), DIC,  $C_{pre}$  and  $C_{sat}$  in the Atlantic between 500 and 2,000 m depth show small vertical gradients and relatively low concentrations, in contrast to the Pacific, Indian and Southern Oceans. As a result of the AMOC shut-down, the North Atlantic stratifies and becomes more like the North Pacific, which leads to increases of DIC,  $C_{pre}$  and  $C_{sat}$  in that depth range in the Atlantic. The increase in DIC is largest ( $\sim 160 \text{ mmol/m}^3$ ) at 2 km depth, dominated by  $C_{pre}$  ( $\sim 80 \text{ mmol/m}^3$ ), but  $C_{soft}$  ( $\sim 50 \text{ mmol/m}^3$ ) and  $C_{caco3}$  ( $\sim 20 \text{ mmol/m}^3$ ) contributions are also important.  $C_{sat}$  contributes substantially to the increase in the upper 3 km. Note that the difference between  $C_{sat}$  and  $C_{pre}$  is the disequilibrium carbon, which dominates changes in  $C_{pre}$ .

In response to the collapse of the AMOC, DIC,  $C_{pre}$  and  $C_{sat}$  decreased in the Pacific, Indian, and Southern Oceans (Figure 6d). In these oceans, the decreases have a peak around 1.5 km depth, and the decreases are smaller in magnitude than their respective counterparts in the Atlantic. Preformed carbon changes dominate changes in DIC in the Pacific, Indian, and Southern Oceans, explaining about two-thirds of the peak around 1.5 km depth.  $C_{soft}$  contributes less than one third to the decrease in the upper ocean and does not change significantly in the deep ocean, while  $C_{caco3}$  increases slightly in the deep ocean. Disequilibrium changes dominate the decrease in preformed carbon outside of the Atlantic at year 4000, although saturation carbon changes are still substantial and were larger earlier in the simulation around year 1500 (Figure 5).

The sum of the components  $\Sigma$  accurately reproduces the mean changes in DIC throughout the ocean basins, both inside and outside the Atlantic. In contrast, the AOU approximation overestimates changes in  $C_{soft}$  particularly in the deep Pacific, Indian, and Southern Oceans, where  $C_{soft}$  changes are close to zero, while  $C_{soft,AOU}$  shows a decrease of approximately  $10 \text{ mmol/m}^3$ .

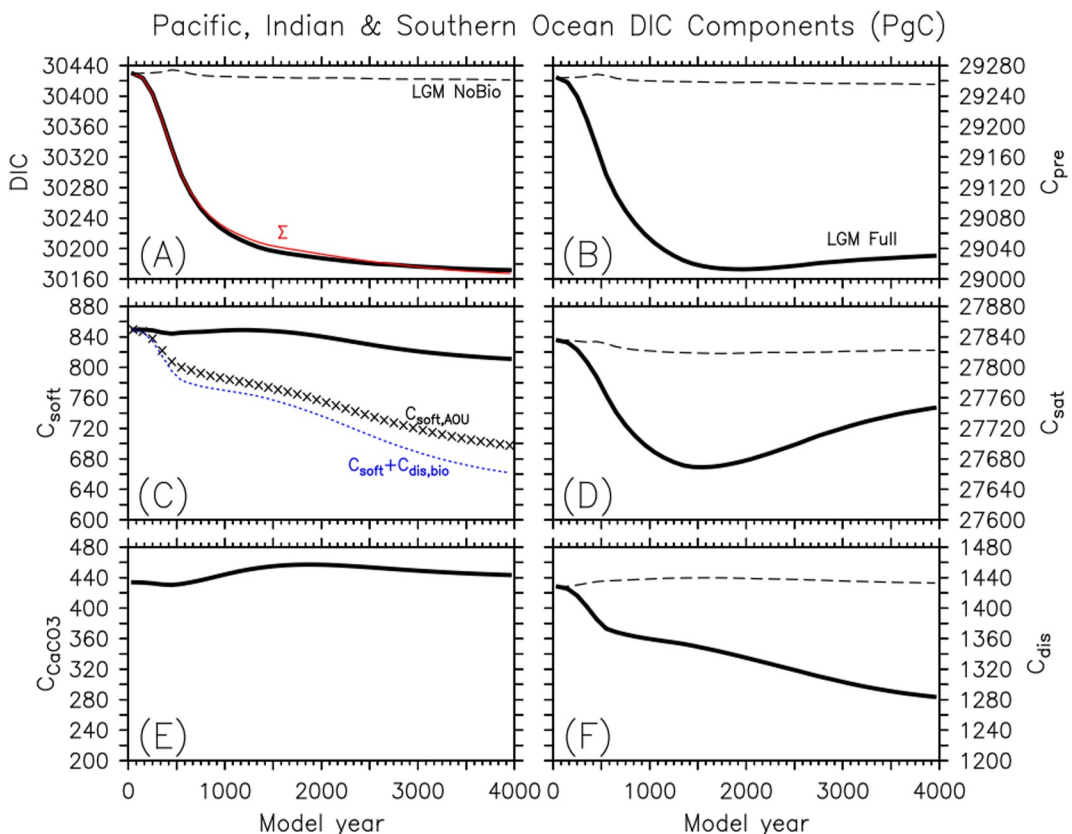


**Figure 5.** As Figure 4 but for Pacific, Indian and Southern Oceans including the Atlantic south of 40°S.  $\Sigma(t = 0) = 30,547 \text{ Pg}$ ,  $C_{phy}(t = 0) = C_{pre,phy}(t = 0) = 28,228 \text{ Pg}$ ,  $C_{soft,AOU}(t = 0) = 2,076 \text{ Pg}$ ,  $C_{sat,phy}(t = 0) = 28,820 \text{ Pg}$ ,  $C_{dis,phy}(t = 0) = -324 \text{ Pg}$ .

The increase in DIC in the Atlantic is focused at depths of  $\sim 2,000 \text{ m}$  between  $30^\circ$  and  $60^\circ\text{N}$  with amplitudes of up to  $260 \text{ mmol/m}^3$  (Figure 7). At that depth, the positive anomaly extends south across the equator to about  $50^\circ\text{S}$ , while decreasing in magnitude. Changes are much smaller and negative in the Indian, Pacific and Southern Oceans, exceeding  $-40 \text{ mmol/m}^3$  only in the far North Pacific around  $1 \text{ km}$  depth due to reduced stratification and deeper mixed layers there, consistent with previous simulations (Schmittner et al., 2007). The large difference in DIC concentrations between the North Atlantic and the North Pacific above  $\sim 3 \text{ km}$  depth in year 0 (panels d and g in Figure 7), which is due to differences in deep water formation, is erased by the AMOC shutdown (panels e and h in Figure 7).

The errors of the decomposition  $\epsilon = \Sigma - \text{DIC}$  are largest in the deep North Atlantic and North Pacific, exceeding  $20 \text{ mmol/m}^3$  (Figures 8a, 8d, and 8g). However, this corresponds to less than 1% of the DIC concentrations there, indicating that the decomposition is accurate. The errors do not change much during the course of the simulation (Figure 8). The greatest changes occur in the North Atlantic around  $3 \text{ km}$  deep, where  $\Sigma$  increases by up to  $15 \text{ mmol/m}^3$ . Compared with the amplitude of the DIC changes of around  $200 \text{ mmol/m}^3$  there, the error is less than 10%. In most of the ocean, the changes in  $\Sigma$  are less than  $\pm 5 \text{ mmol/m}^3$ .

#### 4.2.1. Regenerated Components

The distribution of remineralized carbon in model year 0 is characterized by maxima at the equator around  $500 \text{ m}$  depth and in the North Pacific around  $1,500 \text{ m}$ , while concentrations in the North Atlantic at that depth are very small (Figures 9a, 9d, and 9g). The latter, of course, is due to the formation of deep water in the North Atlantic, where the advection of surface waters with little  $C_{soft}$  causes low values at depth, while the waters of the North Pacific have accumulated respired carbon during a long subsurface travel time. The collapse of the AMOC leads to a large increase in respired carbon in the North Atlantic (Figures 9c and 9f). Concentrations between  $1.5$  and  $2.5 \text{ km}$  depth increase by up to  $100 \text{ mmol/m}^3$ , resembling the pattern of changes in DIC (Figure 7f) and

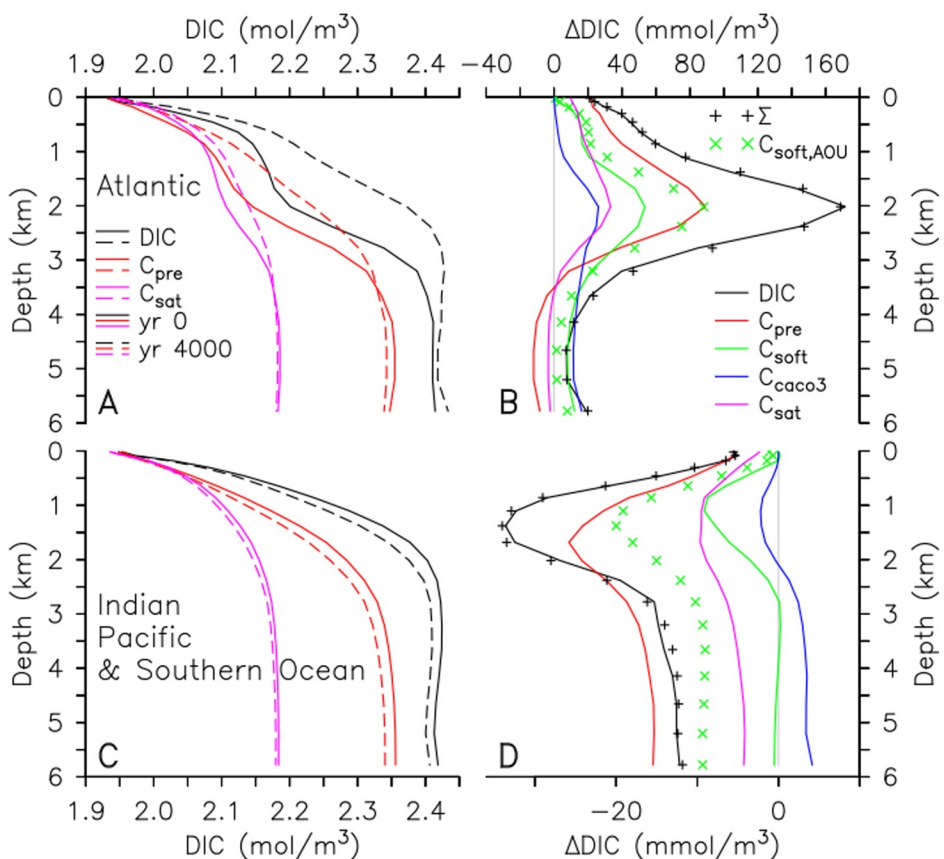


**Figure 6.** Horizontally averaged carbon components in the Atlantic (a, b) and Indian, Pacific and Southern Oceans (c, d). (a) and (c) show absolute values of DIC (black),  $C_{pre}$  (red) and  $C_{sat}$  (purple) at years 0 (solid, AMOC on) and 4000 (dashed, AMOC off). (b) and (d) show differences (yr 4000 minus yr 0) for DIC (black),  $C_{pre}$  (red),  $C_{soft}$  (green),  $C_{caco_3}$  (blue),  $C_{sat}$  (purple),  $\Sigma$  (black symbols) and  $C_{soft,AOU}$  (green symbols).

presenting an important contribution to the DIC changes there. In the North Pacific  $C_{soft}$  decreases by up to 20 mmol/m<sup>3</sup>, also contributing substantially to the loss of DIC there (panel i in Figures 7 and 9).

Owing to the deeper dissolution of CaCO<sub>3</sub> compared to soft-tissue organic matter remineralization, maxima of  $C_{caco_3}$  are located below 3 km depth in the North Atlantic and North Pacific (Figure 10). The AMOC shutdown leads to less dramatic changes in the Atlantic than for  $C_{soft}$ , although a similar pattern with a maximum of more than 40 mmol/m<sup>3</sup> around 2.5 km depth, which contributes significantly to the increases in DIC there. Changes in the Pacific are negligible.

#### 4.2.2. Preformed Components

Preformed carbon concentrations are largest in deep waters of southern origin (Figure 11). Since deep water in the North Atlantic is advected from surface waters with much lower preformed carbon concentrations, at year 0  $C_{pre}$  is much lower in the upper North Atlantic than in the North Pacific. The AMOC collapse decreases these differences. As a result, preformed carbon concentrations in the North Atlantic around 2 km depth increase by more than 120 mmol/m<sup>3</sup>, whereas they decrease in much of the Indian and Pacific oceans by a smaller magnitude (20–40 mmol/m<sup>3</sup>). Preformed carbon is thus the dominant contribution to DIC changes, both in the Atlantic and Pacific.

The biological disequilibrium is largest in waters from the Southern Ocean, where it contributes up to 220 mmol/m<sup>3</sup> to elevated concentrations of preformed carbon (Figure 12). At year 0,  $C_{dis,bio}$  is lower in the deep North Atlantic than in the North Pacific. As a response to the decline in AMOC,  $C_{dis,bio}$  increases in the North Atlantic by up to 80 mmol/m<sup>3</sup>, explaining about half of the increase in preformed carbon there, while it decreases

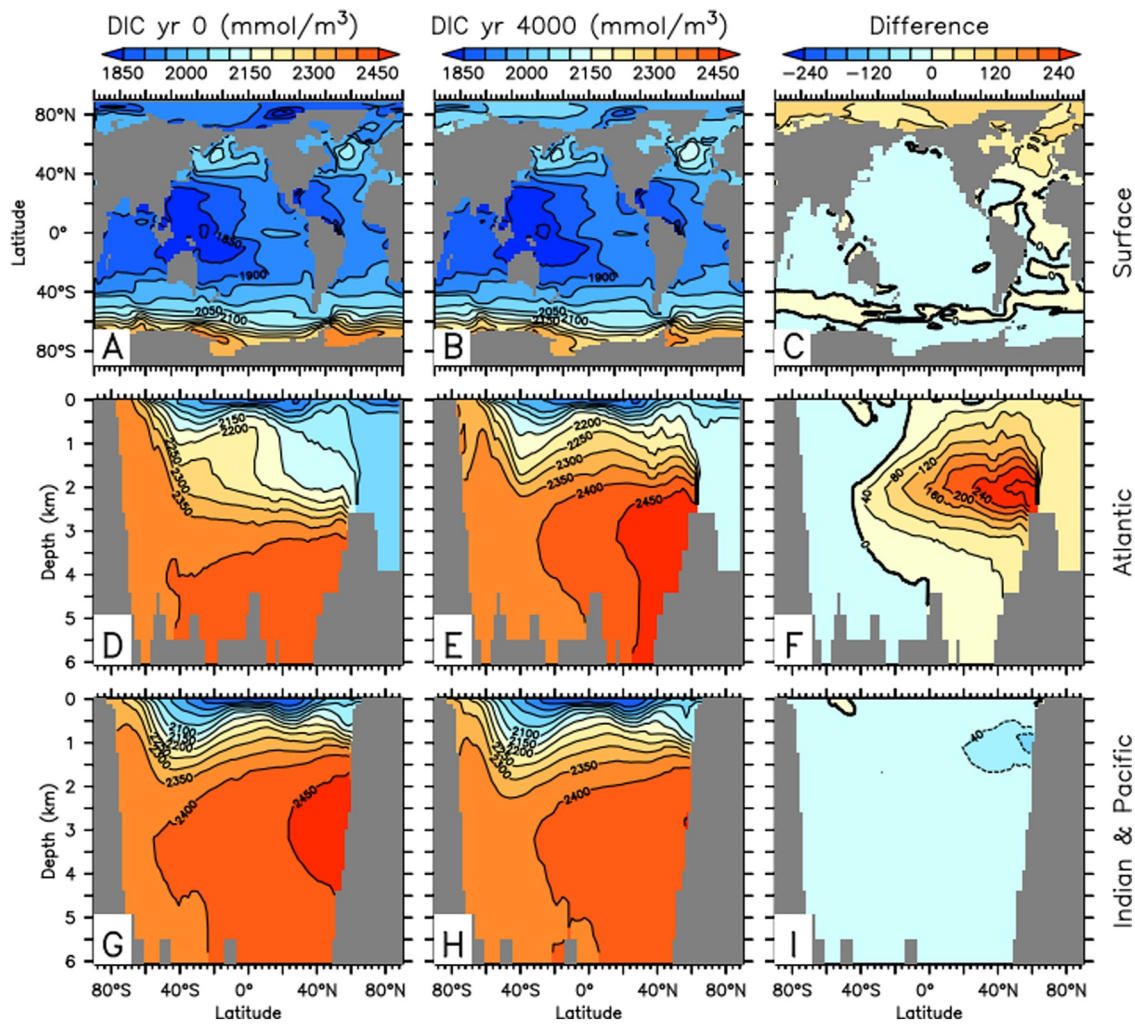


**Figure 7.** Dissolved Inorganic Carbon (DIC) distributions at the surface (a–c) and zonally averaged sections in the Atlantic (d–f) and Indian/Pacific (g–i) in model Full at year 0 (a, d, g), at year 4000 (b, e, h), and the difference (year 4000 minus year 0, c, f, i).

in the Pacific, Indian and Southern Oceans by up to 20 mmol/m<sup>3</sup>. The biological disequilibrium is sensitive to Southern Ocean sea ice cover (Khatiwala et al., 2019). Sea ice prevents outgassing of biologically sequestered carbon and thereby increases  $C_{dis,bio}$ . The AMOC collapse in model *LGM Full* leads to warming of the Southern Ocean due to reduced northward heat transport (Crowley, 1992) and thus a reduction of Southern Ocean sea ice area by ~10%. This could explain the decrease in biological disequilibrium carbon storage in the Southern Ocean and deep Indian and Pacific. On the other hand, a reduction in sea ice cover could also be expected to increase (decrease the magnitude of) the physical disequilibrium, but  $C_{dis,phy}$  changes are much smaller than those of  $C_{dis,bio}$  (Figure S2 in Supporting Information S1). A precise attribution of different forcing factors requires dedicated experiments with an offline model (Khatiwala et al., 2019), which is beyond the scope of this paper.  $C_{dis,bio}$  accounts for nearly all the changes in the total disequilibrium ( $C_{dis}$ , Figure S1 in Supporting Information S1). Biological saturation carbon changes are smaller, contributing up to 50 mmol/m<sup>3</sup> in the North Atlantic and –10 mmol/m<sup>3</sup> in the upper Pacific (Figure 13).

$C_{sat,bio}$  changes are strongly influenced by changes in preformed biological alkalinity (Figure 14),  $ALK_{pre,bio} = ALK - 2 \times C_{caco_3} - ALK_{NoBio}$ , since the saturation concentration of DIC ( $DIC_{sat} = DIC(T, S, ALK, pCO_{2,atm})$ ) depends on alkalinity. Biology removes alkalinity from the surface through the production of  $CaCO_3$  and redistributes it in the deep ocean, which is why  $ALK_{pre,bio}$  is negative at the surface. The amount of alkalinity redistributed is twice the amount of carbon, hence the factor of two in the above equation (Zeebe &

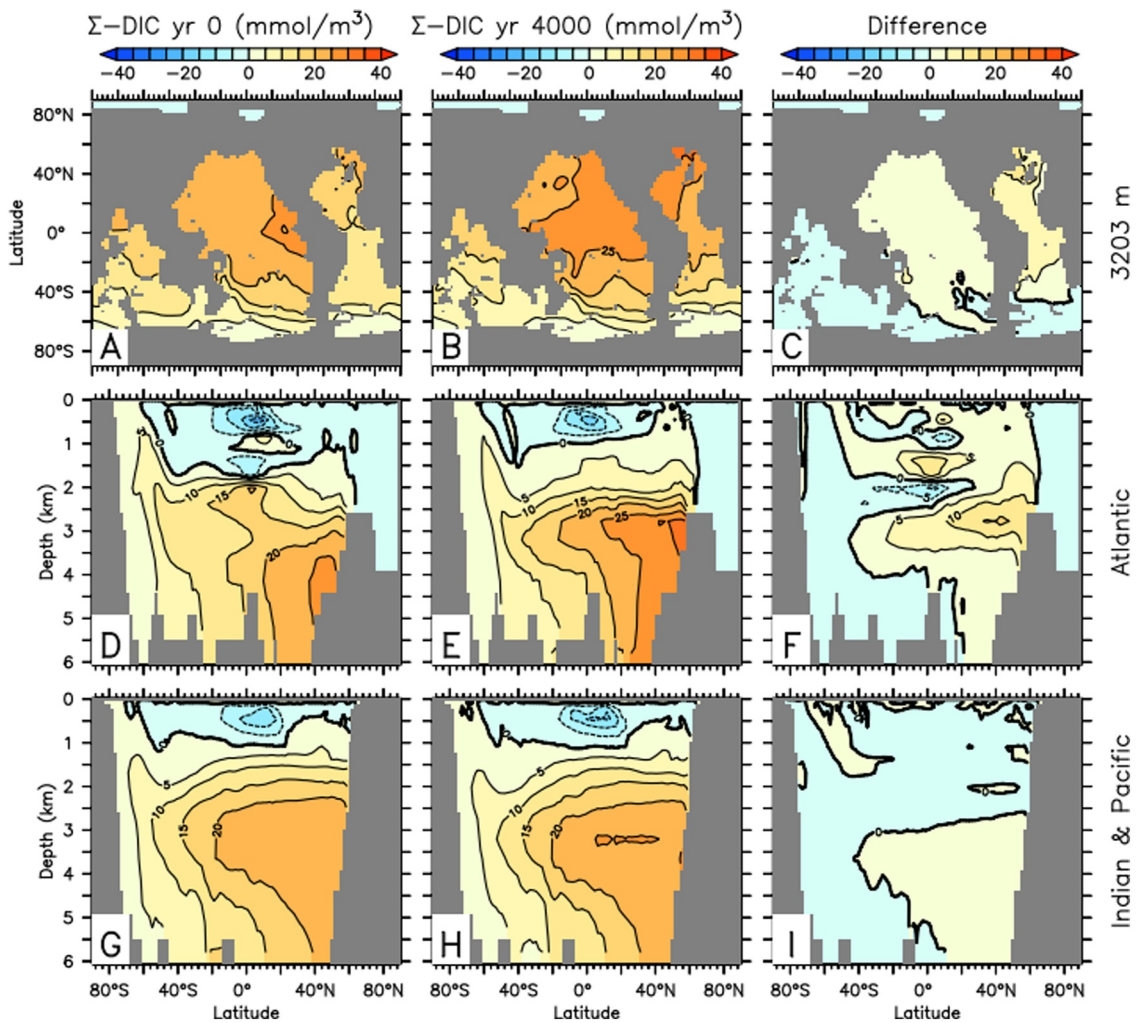


**Figure 8.** As Figure 7 but for error of decomposition ( $\epsilon = \Sigma - \text{DIC}$ ). Top row shows maps at 3,203 m depth close to the maximum error in (f). Note different range of color scale compared with Figure 7.

Wolf-Gladrow, 2001). Since  $\text{ALK}_{\text{pre},\text{bio}}$  is a conserved quantity with no sources in the interior, its negative surface values are advected into the interior. In response to the collapse of the AMOC,  $\text{ALK}_{\text{pre},\text{bio}}$  increases in the North Atlantic, which increases  $C_{\text{sat},\text{bio}}$  there (Figure 13). At year 0,  $\text{ALK}_{\text{pre},\text{bio}}$  is lower in the surface waters of the North Atlantic and at the depth of North Atlantic Deep Water than in the North Pacific and Southern Ocean. This may be due to the advection of low-alkalinity waters from the tropics to the North Atlantic by the AMOC. A reduction in AMOC would reduce this advection, increase  $\text{ALK}_{\text{pre},\text{bio}}$  in the surface waters of the North Atlantic, and thus increase  $C_{\text{sat},\text{bio}}$  there as well. Note that  $C_{\text{sat},\text{bio}}$  would also be influenced by differences in atmospheric CO<sub>2</sub> between models *LGM Full* and *LGM NoBio*. However, this effect is likely not associated with distinct spatial patterns. Rather, it would lead to a uniform change in  $C_{\text{sat},\text{bio}}$  across the ocean. Moreover,  $C_{\text{sat},\text{bio}}$  could be affected by the relatively small differences in temperature and salinity between these experiments, but this effect is likely to be small.

Changes in physical disequilibrium (Figure S2 in Supporting Information S1) are much smaller than those in biological disequilibrium, contributing less than 15 mmol/m<sup>3</sup> in the North Atlantic and less than 5 mmol/m<sup>3</sup> elsewhere. Physical saturation changes are mostly confined to the near-surface Atlantic, where they are  $\sim 10$  mmol/m<sup>3</sup> (Figure S3 in Supporting Information S1).  $C_{\text{sat},\text{phy}}$  changes in the deep ocean are negligible.

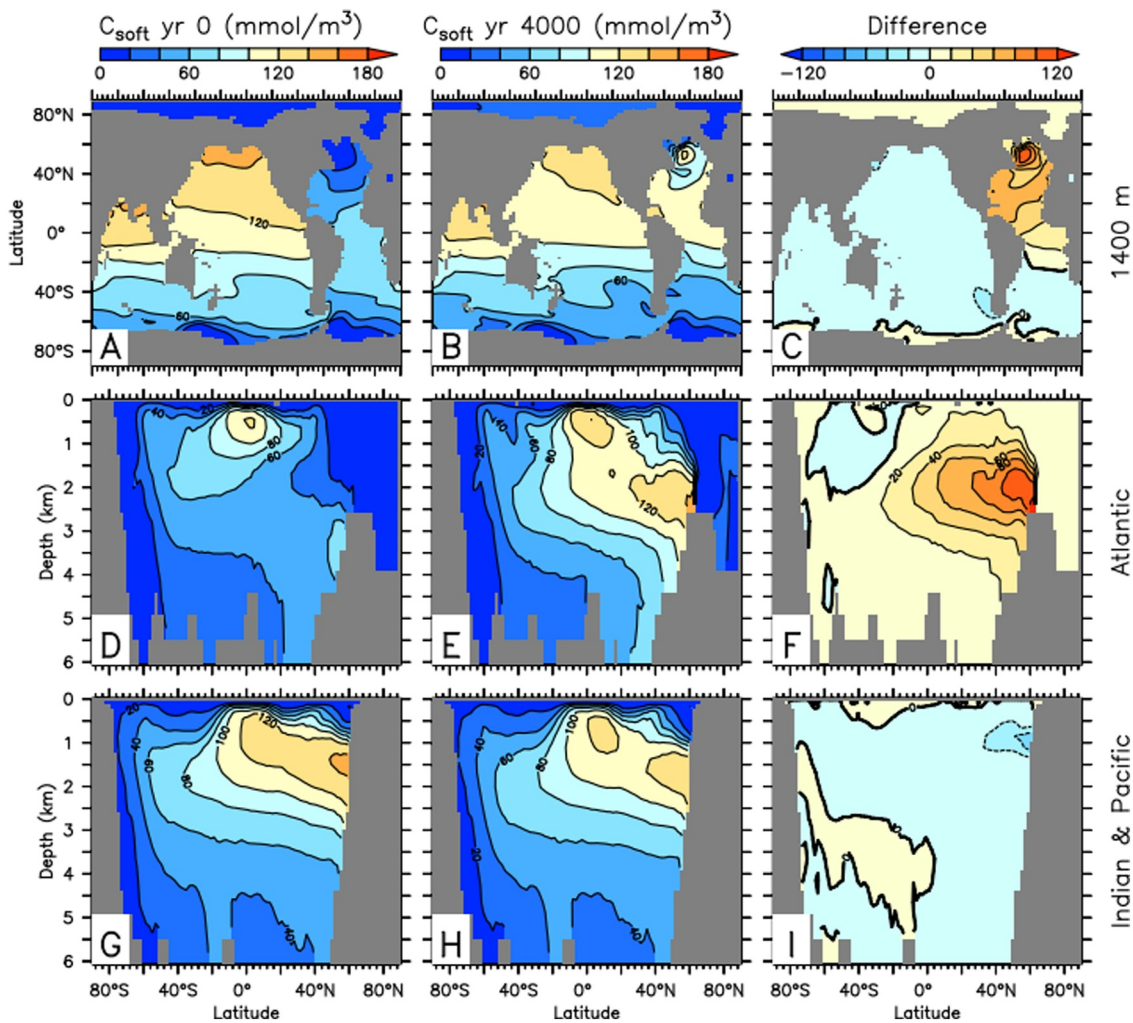


**Figure 9.** As Figure 7 but for remineralized soft-tissue carbon ( $C_{soft}$ ). Top row shows maps at 1,400 m. Note different range of color scale compared with Figure 7.

## 5. Simulations of AMOC Collapse Under Preindustrial Climate

The response of the carbon cycle to changes in AMOC depends on the background climate conditions. Consistent with previous results (Menkveld et al., 2008; Schmittner et al., 2007), applying the same freshwater forcing to a preindustrial simulation in model *PI Full* leads to much larger changes (Figures S4 and S5 in Supporting Information S1). Since the AMOC is stronger and deeper in model *PI Full* than in model *LGM Full* at year 0 (Figure 2 vs. Figure S4 in Supporting Information S1) its shut-down has bigger effects. Atmospheric CO<sub>2</sub> shows a qualitatively similar response to *LGM Full* with an initial decrease during the first 500 years, followed by a slow increase, but the amplitude of the changes is larger such that in year 4000 CO<sub>2</sub> is approximately 20 ppm higher than in year 0 and 27 ppm higher than in year 500 (Figure S5 in Supporting Information S1 vs. Figure 1).

The response of land carbon is positive throughout the simulation, in contrast to *LGM Full*, presumably due to larger changes in atmospheric CO<sub>2</sub>. Ocean carbon decreases by about 100 Pg by year 4000, in contrast to the change of  $\sim$ 20 Pg in model *LGM Full*. The response of the global carbon components is quite different from that in model *LGM Full* (Figure S6 in Supporting Information S1 vs. Figure 3).  $C_{soft}$  decreases over the full course of the simulation, consistent with Schmittner and Lund (2015), whereas in model *LGM Full* it increases.  $C_{pre}$  increases, whereas in model *LGM Full* it decreases. The reason for these qualitatively different responses of the global components is related to the fact that they are small residuals of larger inter-basin redistributions. Regenerated and preformed carbon components still increase in the Atlantic, as in model *LGM Full*, but the changes are larger and more gradual (Figure S7 in Supporting Information S1 vs. Figure 4). In the Atlantic, the peak in the

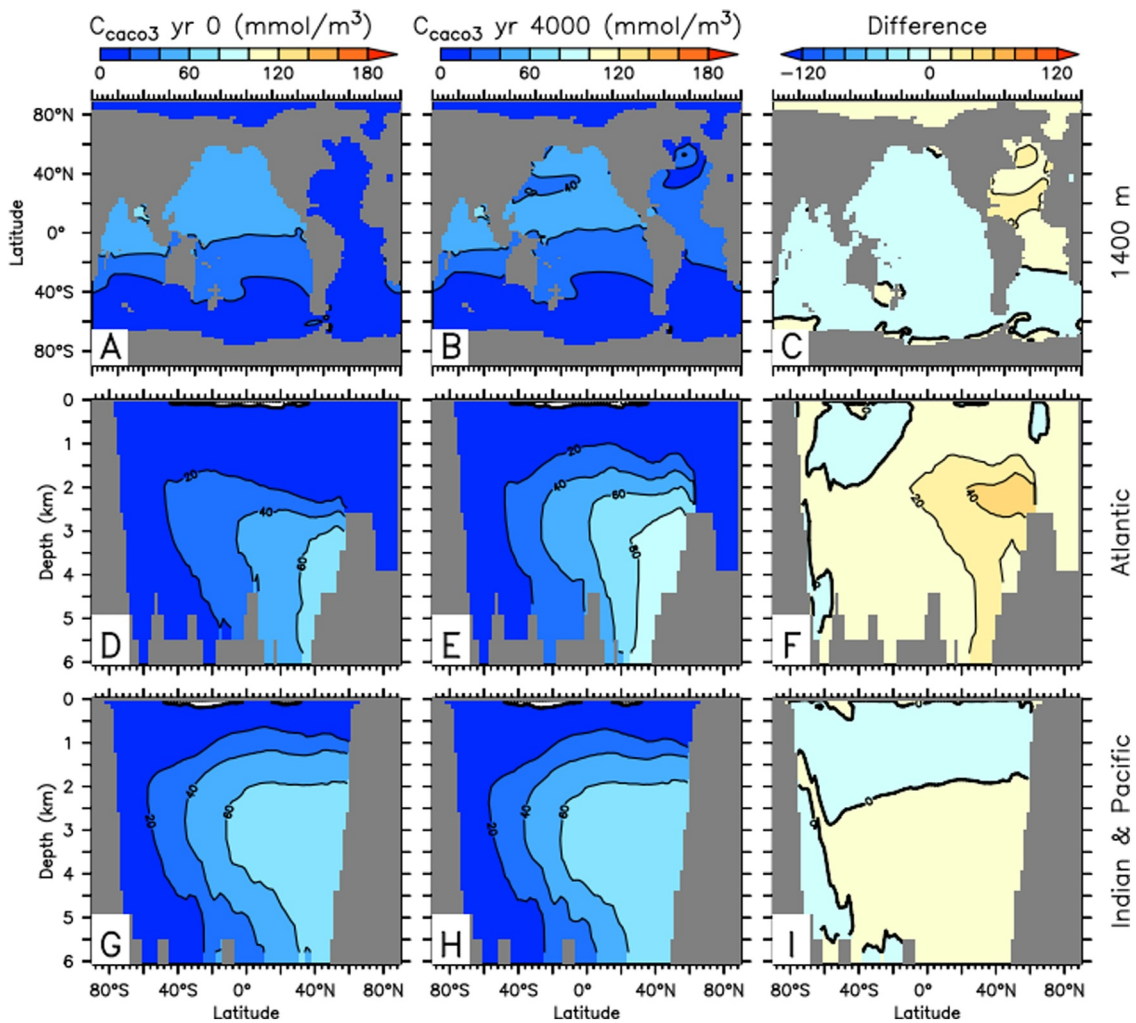


**Figure 10.** As Figure 9 but for dissolved  $\text{CaCO}_3$  carbon ( $C_{\text{caco}_3}$ ).

DIC increase is broader, extends over a larger depth range and is impacted by a larger contribution of  $C_{\text{soft}}$ , particularly in the upper 1 km (Figure 6 vs. Figure 15).

A crucial factor for the decrease in global ocean carbon is the substantial loss ( $-293 \text{ Pg by yr 4000}$ ) of remineralized carbon in the Pacific, Indian and Southern Oceans (Figure S8 in Supporting Information S1), in contrast to the small changes ( $-38 \text{ Pg}$ ) there in *LGM Full* (Figure 5). Together with the decrease in  $-108 \text{ Pg}$  in  $C_{\text{caco}_3}$ , this reduces the DIC in the Pacific, Indian, and Southern Oceans by  $-401 \text{ Pg}$ , exceeding the total increase in DIC of  $368 \text{ Pg}$  in the Atlantic.

The vertical distribution of the DIC loss in the Pacific, Indian, and Southern Oceans (Figure 15) is similar to that in model *LGM Full* (Figure 6) with a peak around 1.5 km depth and smaller decreases below 2.5 km. However, the magnitude in *PI Full* is larger and rather than being dominated by  $C_{\text{pre}}$ , it is dominated by  $C_{\text{soft}}$ , which shows a fairly uniform decrease below about 1 km depth.

The muted response in preformed carbon in the Pacific, Indian, and Southern Oceans in *PI Full* ( $-14 \text{ Pg}$ ) versus *LGM Full* ( $-233 \text{ Pg}$ ) deserves further exploration. Inspection of spatial patterns reveals that while in *LGM Full* the Indian, Pacific and Southern Oceans show negative anomalies throughout, in *PI Full*  $C_{\text{pre}}$  increases in the Southern Ocean and below 2.5 km in the Pacific and Indian oceans (Figures S12 and S11 in Supporting Information S1). This pattern in *PI Full* is dominated by changes in  $C_{\text{sat}}$  (Figure S13 in Supporting Information S1), while disequilibrium changes are much smaller in the Indian and Pacific oceans (Figure S14 in Supporting

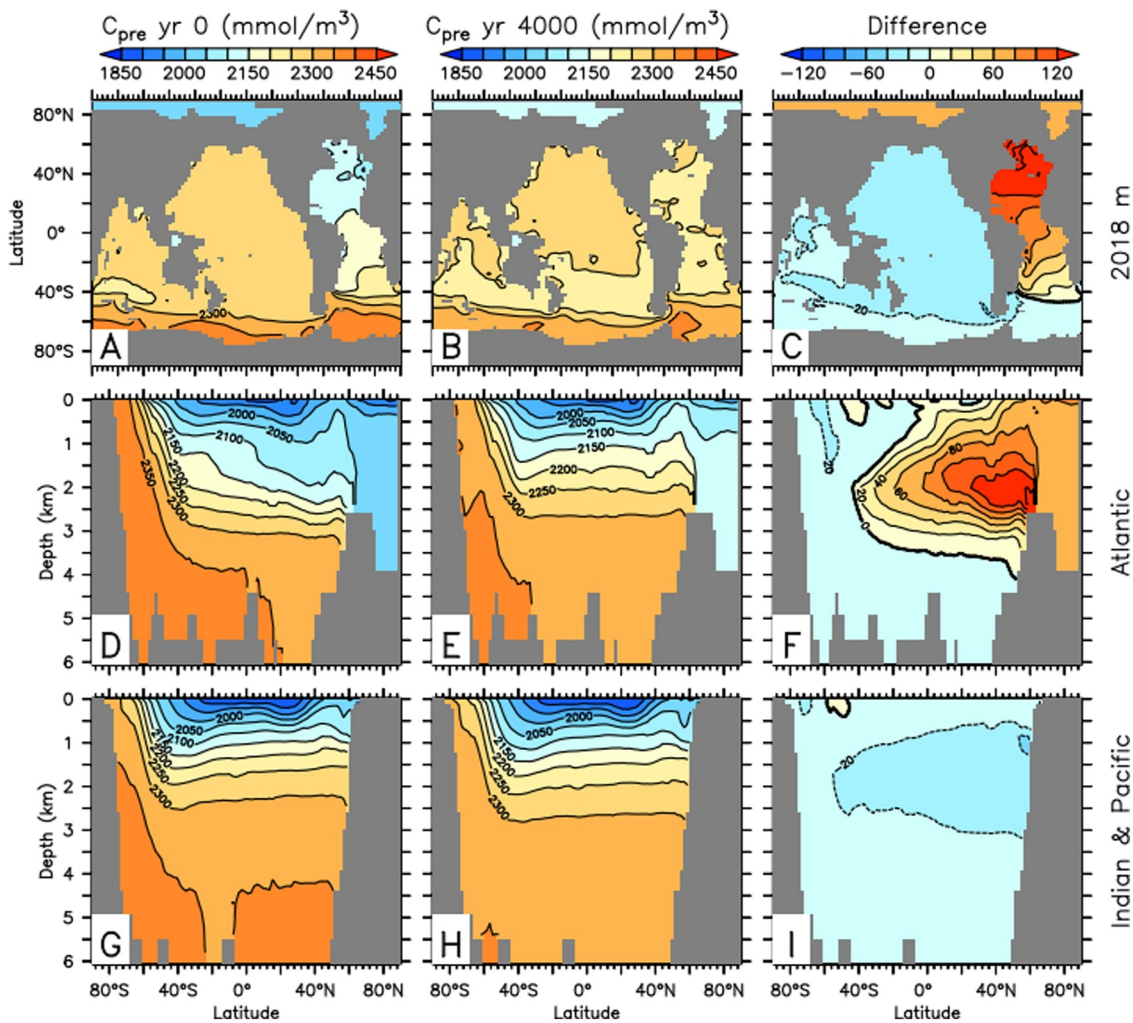


**Figure 11.** As Figure 9 but for preformed carbon ( $C_{pre}$ ).

Information S1). We hypothesize that disequilibrium changes in the deep Indian and Pacific oceans are smaller in *PI Full*, because its deeper and stronger AMOC at year 0 injects waters with low  $C_{dis}$  into the Southern Ocean, from where it flows into the deep Indian and Pacific and impacts  $C_{dis}$  there. In contrast, in *LGM Full* the AMOC is shallower and does not impact the deep Indian and Pacific as much. Thus, in *PI Full* the AMOC collapse causes an increase of disequilibrium carbon in the deep Indian and Pacific, relative to that in *LGM Full*. Both are influenced by the sea ice reduction, which decreases the magnitude of  $C_{dis,bio}$ .

The AOU approximation of  $C_{soft}$  suggests a decrease of more than 400 Pg (Figure S6 in Supporting Information S1), similar to a previous study (Schmittner & Lund, 2015). However, our precise calculation shows that this overestimates the true changes of 250 Pg by about 60%. The AOU approximation also overestimates changes in  $C_{soft} + C_{dis,bio}$ . Although changes in  $C_{soft}$  are well captured by the AOU approximation in the Atlantic (Figure S7 in Supporting Information S1), in the Pacific they are overestimated by about 100 Pg or one-third (Figure S8 in Supporting Information S1, Figure 15).

## 6. Discussion

Although the AOU approximation overestimates the changes in  $C_{soft}$  in model *PI Full*, the changes in  $C_{soft}$  are still dominant in the global DIC loss in this experiment, consistent with previous conclusions using the AOU approximation (Schmittner & Lund, 2015). However, in *LGM Full*, preformed carbon changes dominate the global ocean DIC decrease and most regional changes. Nevertheless, even in that case, the biological components

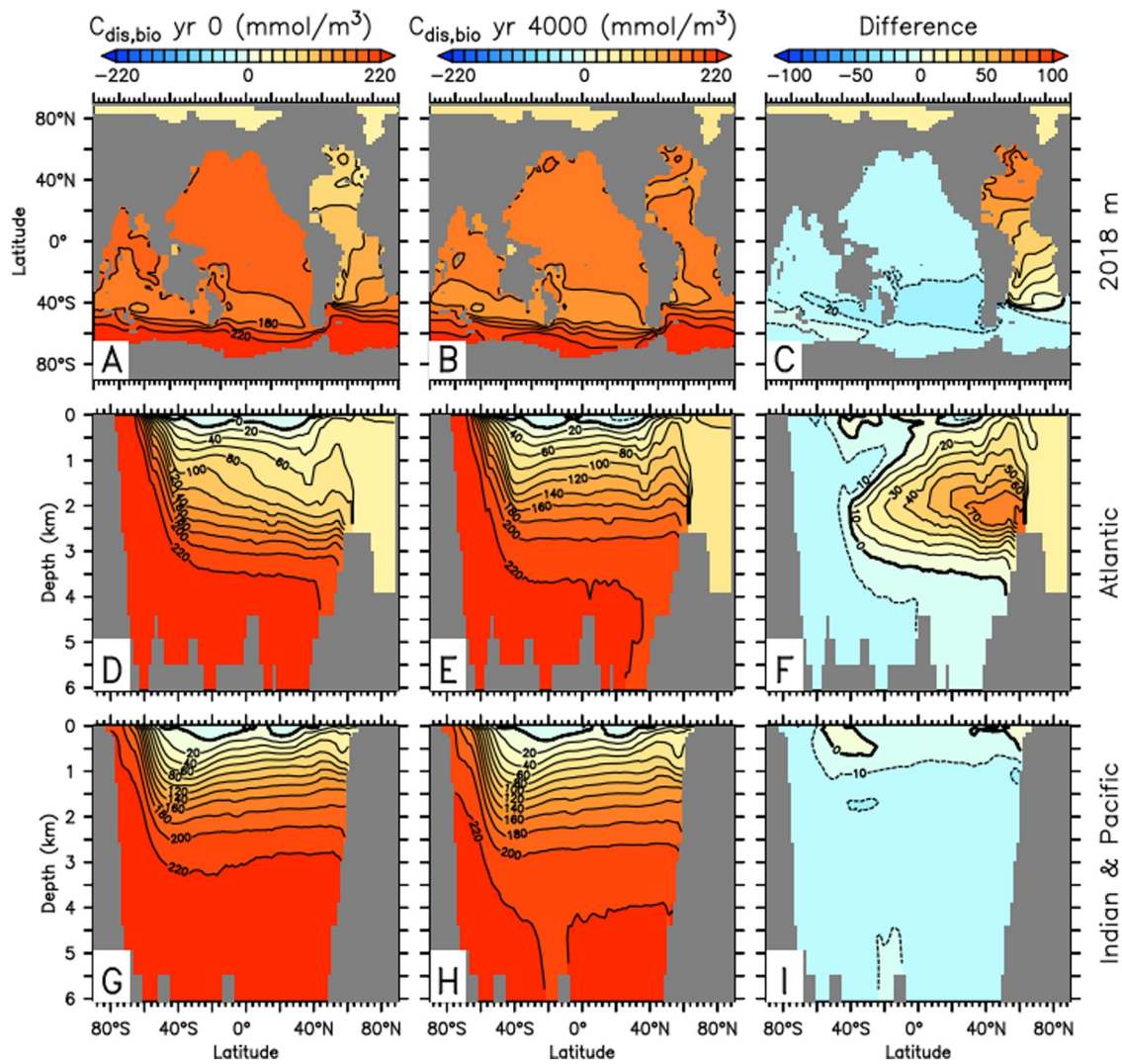


**Figure 12.** As Figure 9 but for biological disequilibrium carbon ( $C_{dis,bio}$ ).

of preformed carbon  $C_{dis,bio}$  and  $C_{sat,bio}$  determine changes in  $C_{pre}$ . Thus, in both cases, changes in ocean circulation affect global ocean carbon storage primarily through biological carbon, consistent with previous conclusions (Schmittner & Galbraith, 2008; Schmittner & Lund, 2015). However, the decomposition provides additional information regarding the precise mechanisms of biological carbon changes. For example, a mechanism that has previously not been considered is that of biological saturation carbon ( $C_{sat,bio}$ ) changes, which dominate changes in preformed carbon over the first 2000 years of the *LGM Full* simulation (Figure 3). This component is affected by changes in surface alkalinity (Figures 13 and 14). The spatial patterns of the  $C_{sat,bio}$  and  $ALK_{pre,bio}$  anomalies in year 1500 are similar to those at year 4000, but the negative anomalies outside the Atlantic are larger (not shown). Upper ocean alkalinity decreases outside the Atlantic in response to an AMOC shutdown due to reduced upwelling of high-alkalinity deep waters to the surface. This is similar to the response of nutrients (Schmittner, 2005) and the analysis of the effects of alkalinity on future carbon uptake (Chikamoto et al., 2023). Reduced productivity and calcium carbonate production then leads to a slow partial recovery of upper ocean nutrients and alkalinity, causing an increase in  $C_{sat,bio}$  after the year 1500.

Although the decomposition has systematic errors (Figure 8) those errors are small and do not change much over time. Basin-wide changes in DIC are approximated with high accuracy (Figures 4–6). Locally and globally, biases can be more significant (Figures 3 and 8). Nevertheless, errors of the decomposition are typically in the single-digit percent range such that, for most applications, the decomposition will yield reliable and accurate results. We

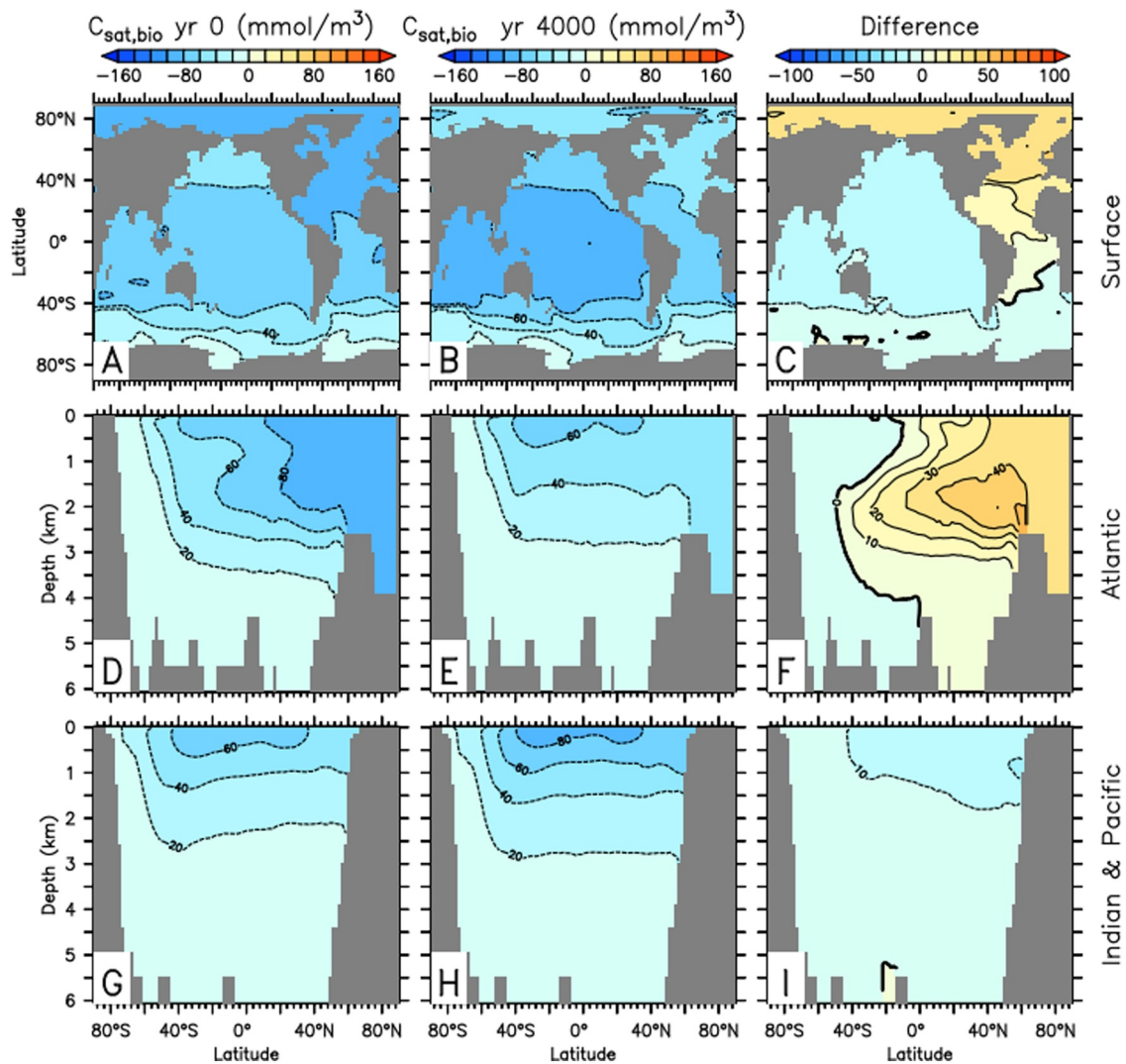


**Figure 13.** As Figure 9 but for biological saturation carbon ( $C_{sat,bio}$ ).

also note that the decomposition is complete in that it estimates the regenerated and preformed components independently and does not leave one component to be estimated as a residual, in contrast to previous approaches (Eggleston & Galbraith, 2018; Gruber et al., 1996; Schmittner et al., 2013). Separating biological from physical contributions helps to interpret the results.

Our results have implications for future projections, which include the possibility of an AMOC shutdown (Rahmstorf, 2024). We would expect many similarities with the simulations presented here, such as the redistribution of regenerated and preformed carbon, but also a number of differences. Since our simulations don't include anthropogenic carbon increases and the associated warming we can expect differences due to those factors. For example, warming can be expected to affect the physical saturation carbon more than in the simulations presented here. More work is needed, combining anthropogenic carbon emissions with an AMOC collapse scenario, to quantify these contributions.

## 7. Conclusions

We conclude that the decomposition of the ocean carbon components is complete and accurate even in transient simulations and therefore supports the previous results from equilibrium simulations (Khatiwala et al., 2019; Schmittner & Fillman, 2024). This is in contrast to the results from the AOU approximation of  $C_{soft}$ , which often leads to large errors and is generally not reliable (Figures 3–6). This is not surprising given the fact that the AOU

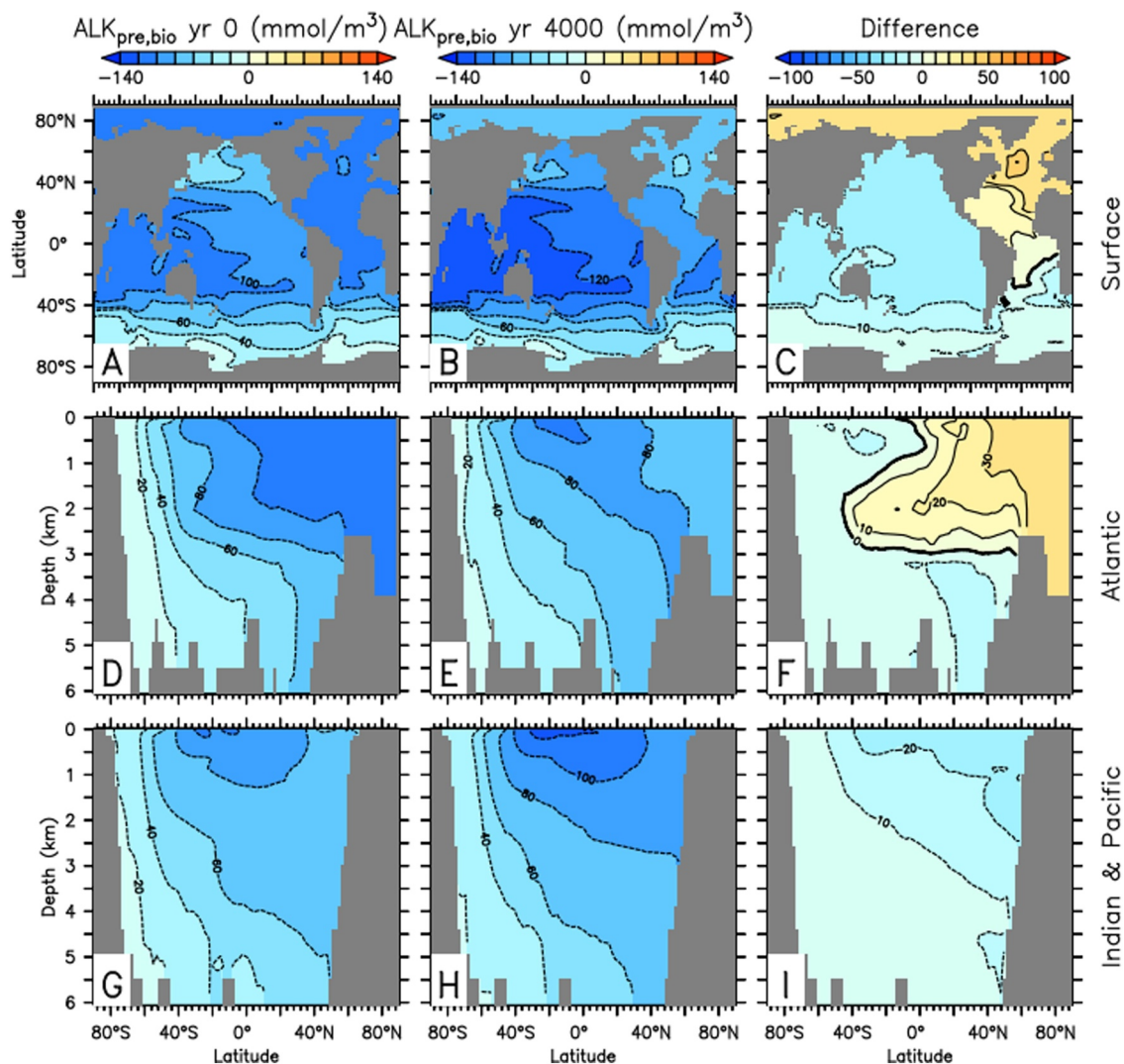


**Figure 14.** As Figure 12 but for preformed biological alkalinity, which is calculated as alkalinity in model *LGM Full* minus  $2 \times C_{caco_3}$  minus alkalinity in model *LGM NoBio*.

approximation includes effects of oxygen disequilibrium. The errors of the AOU approximation seem to be smaller for estimating  $C_{soft} + C_{dis,bio}$ , but since the oxygen disequilibrium is different from that of carbon, even this quantity is poorly estimated.

In response to a shutdown of AMOC in an LGM background climate, ocean carbon increases and then decreases, leading to opposite changes in atmospheric CO<sub>2</sub> (Figure 1). The initial increase in DIC is caused by the rapid growth of preformed and regenerated carbon in the Atlantic (Figure 4), while the long-term decrease is dominated by changes in preformed carbon outside the Atlantic (Figure 5). Although preformed carbon changes are mostly dominated by changes in biological disequilibrium, biological saturation changes are also important. Biological disequilibrium carbon increases in the Atlantic and decreases in the other ocean basins as the AMOC is shut down. The increase in  $C_{dis,bio}$  in the Atlantic is due to the lack of input of North Atlantic Deep Water with low  $C_{dis,bio}$ . The decrease of  $C_{dis,bio}$  in the other ocean basins is likely impacted by a decrease in the sea ice cover in the Southern Ocean. Biological saturation carbon decreases outside the Atlantic are caused by decreases in surface alkalinity due to reduced upwelling of biologically sequestered high-alkalinity deep waters.

If the AMOC shutdown occurs in a preindustrial climate, the ocean and atmospheric carbon changes are larger than in the LGM. Regenerated components are relatively more important, particularly outside the Atlantic, where

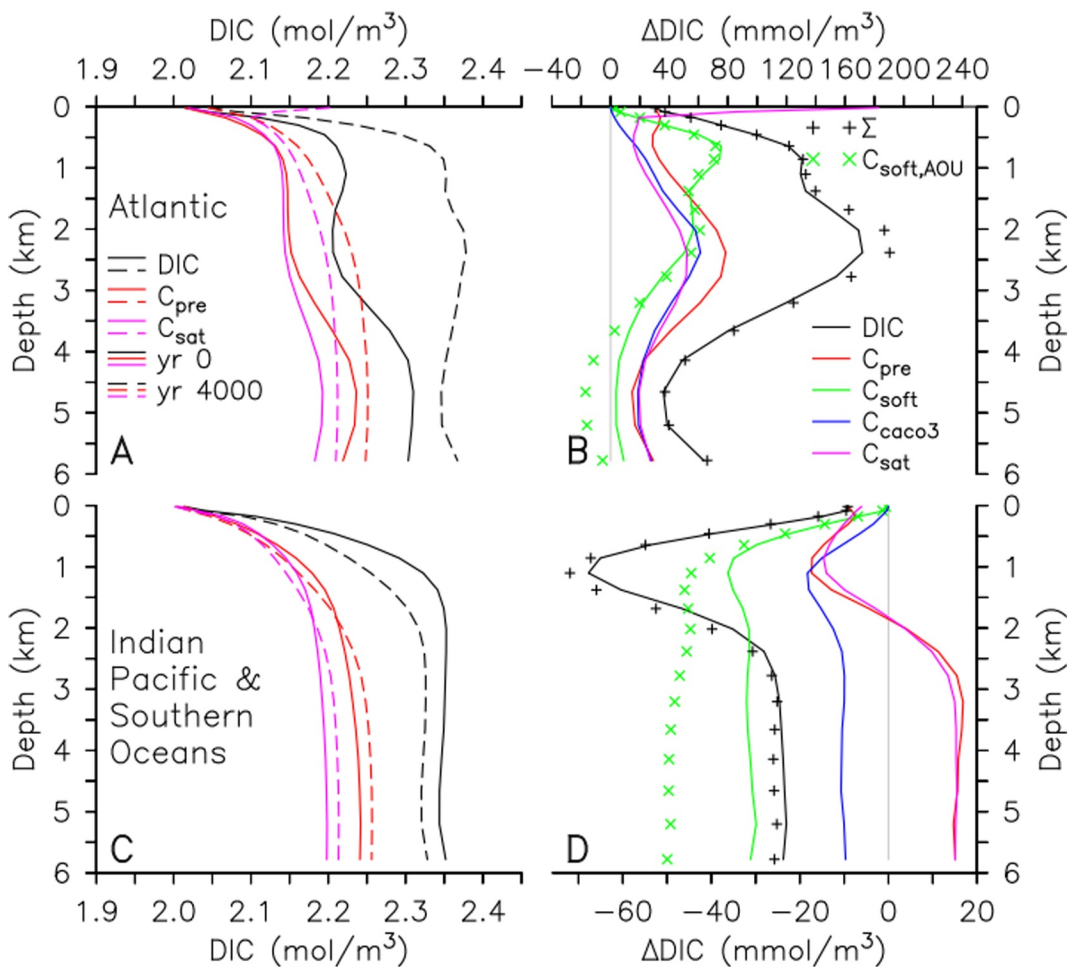


**Figure 15.** Horizontally averaged carbon components in the Atlantic (a, b) and Indian, Pacific and Southern Oceans (c, d) in *PI Full*. (a) and (c) show absolute values of DIC (black),  $C_{pre}$  (red) and  $C_{sat}$  (purple) at years 0 (solid, AMOC on) and 4000 (dashed, AMOC off). (b) and (d) show differences (yr 4000 minus yr 0) for DIC (black),  $C_{pre}$  (red),  $C_{soft}$  (green),  $C_{caco3}$  (blue),  $C_{sat}$  (purple),  $\Sigma$  (black symbols) and  $C_{soft,AOU}$  (green symbols).

$C_{soft}$  and  $C_{caco3}$  decrease, dominating DIC changes (Figure 15). Changes in biologically sequestered carbon dominate changes in ocean carbon in our simulations, regardless of the background climate.

Recent studies have questioned the idea that the AMOC collapsed completely during Heinrich Stadial 1 (Oppo et al., 2015; Pöppelmeier et al., 2023; Repschläger et al., 2021). However, quantifying AMOC changes during this and other past events remains an outstanding task beyond the scope of this paper. The method used here could be applied in the future to data-constrained paleoclimate simulations, which would help better understand past changes in the ocean carbon cycle.

### Conflict of Interest

The authors declare no conflicts of interest relevant to this study.

### Data Availability Statement

The OSU-UVic climate model (version 2.9.10) source code is available on GitHub at <https://github.com/OSU-CEOAS-Schmittner/UVic2.9/releases/tag/v2.9.10> (Schmittner, 2024a). Model code, input and output data, as well as ferret scripts to generate figures from this paper are available at Zenodo for the *LGM Full* model

<https://doi.org/10.5281/zenodo.14231977> (Schmittner, 2024b) and for the *PI Full* model <https://zenodo.org/records/14774855> (Schmittner, 2025b).

## Acknowledgments

AS is grateful for support from the National Science Foundation (NSF) Grant 1924215. We also acknowledge NSF's support of Oregon State University's Research Experiences for Undergraduates Program, which funded MB's research internship at OSU.

## References

- Ahn, J., Brook, E. J., Schmittner, A., & Kreutz, K. (2012). Abrupt change in atmospheric CO<sub>2</sub> during the last ice age. *Geophysical Research Letters*, 39(18), L18711. <https://doi.org/10.1029/2012GL053018>
- Annan, J. D., Hargreaves, J. C., & Mauritsen, T. (2022). A new global surface temperature reconstruction for the Last Glacial Maximum. *Climate of the Past*, 18(8), 1883–1896. <https://doi.org/10.5194/cp-18-1883-2022>
- Archer, D., Kheshtgi, H., & Maier-Reimer, E. (1998). Dynamics of fossil fuel CO<sub>2</sub> neutralization by marine CaCO<sub>3</sub>. *Global Biogeochemical Cycles*, 12(2), 259–276. <https://doi.org/10.1029/98GB00744>
- Bakker, P., Schmittner, A., Lenaerts, J. T. M., Abe-Ouchi, A., Bi, D., van den Broeke, M. R., et al. (2016). Fate of the Atlantic Meridional Overturning Circulation: Strong decline under continued warming and Greenland melting. *Geophysical Research Letters*, 43(23), 12252–12260. <https://doi.org/10.1002/2016GL070457>
- Bauska, T. K., Baggenstos, D., Brook, E. J., Mix, A. C., Marcott, S. A., Petrenko, V. V., et al. (2016). Carbon isotopes characterize rapid changes in atmospheric carbon dioxide during the last deglaciation. *Proceedings of the National Academy of Sciences*, 113(13), 3465–3470. <https://doi.org/10.1073/pnas.1513868113>
- Bauska, T. K., Brook, E. J., Marcott, S. A., Baggenstos, D., Shackleton, S., Severinghaus, J. P., & Petrenko, V. V. (2018). Controls on millennial-scale atmospheric CO<sub>2</sub> variability during the Last Glacial Period. *Geophysical Research Letters*, 45(15), 7731–7740. <https://doi.org/10.1029/2018GL077881>
- Buizert, C., Sigl, M., Severi, M., Markle, B. R., Wettstein, J. J., McConnell, J. R., et al. (2018). Abrupt ice-age shifts in southern westerly winds and Antarctic climate forced from the north. *Nature*, 563(7733), 681–685. <https://doi.org/10.1038/s41586-018-0727-5>
- Buizert, C., Sowers, T. A., Niezgoda, K., Blunier, T., Gkinis, V., Harlan, M., et al. (2024). The Greenland spatial fingerprint of Dansgaard–Oeschger events in observations and models. *Proceedings of the National Academy of Sciences*, 121(44), e2402637121. <https://doi.org/10.1073/pnas.2402637121>
- Chen, C., Riley, W. J., Prentice, I. C., & Keenan, T. F. (2022). CO<sub>2</sub> fertilization of terrestrial photosynthesis inferred from site to global scales. *Proceedings of the National Academy of Sciences*, 119(10), e2115627119. <https://doi.org/10.1073/pnas.2115627119>
- Chiang, J. C. H., & Bitz, C. M. (2005). Influence of high latitude ice cover on the marine Intertropical Convergence Zone. *Climate Dynamics*, 25(5), 477–496. <https://doi.org/10.1007/s00382-005-0040-5>
- Chikamoto, M. O., DiNezio, P., & Lovenduski, N. (2023). Long-term slowdown of ocean carbon uptake by alkalinity dynamics. *Geophysical Research Letters*, 50(4), e2022GL101954. <https://doi.org/10.1029/2022GL101954>
- Cliff, E., Khatiwala, S., & Schmittner, A. (2021). Glacial deep ocean deoxygenation driven by biologically mediated air-sea disequilibrium. *Nature Geoscience*, 14(1), 43–50. <https://doi.org/10.1038/s41561-020-00667-z>
- Crowley, T. J. (1992). North Atlantic Deep Water cools the Southern Hemisphere. *Paleoceanography*, 7(4), 489–497. <https://doi.org/10.1029/92PA01058>
- Duteil, O., Koeve, W., Oschlies, A., Bianchi, D., Galbraith, E., Kriest, I., & Matear, R. (2013). A novel estimate of ocean oxygen utilisation points to a reduced rate of respiration in the ocean interior. *Biogeosciences*, 10(11), 7723–7738. <https://doi.org/10.5194/bg-10-7723-2013>
- Eggleson, S., & Galbraith, E. D. (2018). The devil's in the disequilibrium: Multi-component analysis of dissolved carbon and oxygen changes under a broad range of forcings in a general circulation model. *Biogeosciences*, 15(12), 3761–3777. <https://doi.org/10.5194/bg-15-3761-2018>
- Fillman, N., Schmittner, A., & Kvale, K. F. (2023). Variable stoichiometry effects on glacial/interglacial ocean model biogeochemical cycles and carbon storage (preprint). <https://doi.org/10.22541/essoar.169049091.16856096/v1>
- Frierson, D. M. W., Hwang, Y.-T., Fučkar, N. S., Seager, R., Kang, S. M., Donohoe, A., et al. (2013). Contribution of ocean overturning circulation to tropical rainfall peak in the Northern Hemisphere. *Nature Geoscience*, 6(11), 940–944. <https://doi.org/10.1038/ngeo1987>
- Gebbie, G. (2014). How much did Glacial North Atlantic Water shoal? *Paleoceanography*, 29(3), 190–209. <https://doi.org/10.1002/2013PA002557>
- Gottschalk, J., Battaglia, G., Fischer, H., Frölicher, T. L., Jaccard, S. L., Jeltsch-Thömmes, A., et al. (2019). Mechanisms of millennial-scale atmospheric CO<sub>2</sub> change in numerical model simulations. *Quaternary Science Reviews*, 220, 30–74. <https://doi.org/10.1016/j.quascirev.2019.05.013>
- Gruber, N., Sarmiento, J. L., & Stocker, T. F. (1996). An improved method for detecting anthropogenic CO<sub>2</sub> in the oceans. *Global Biogeochemical Cycles*, 10(4), 809–837. <https://doi.org/10.1029/96GB01608>
- Ito, T., Follows, M. J., & Boyle, E. A. (2004). Is AOU a good measure of respiration in the oceans? *Geophysical Research Letters*, 31(17). <https://doi.org/10.1029/2004GL020900>
- Khatiwala, S., Schmittner, A., & Muglia, J. (2019). Air-sea disequilibrium enhances ocean carbon storage during glacial periods. *Science Advances*, 5(6), eaaw4981. <https://doi.org/10.1126/sciadv.aaw4981>
- Lynch-Stieglitz, J. (2017). The Atlantic meridional overturning circulation and abrupt climate change. *Annual Review of Marine Science*, 9(1), 83–104. <https://doi.org/10.1146/annurev-marine-010816-060415>
- Menking, J. A., Shackleton, S. A., Bauska, T. K., Buffen, A. M., Brook, E. J., Barker, S., et al. (2022). Multiple carbon cycle mechanisms associated with the glaciation of Marine Isotope Stage 4. *Nature Communications*, 13(1), 5443. <https://doi.org/10.1038/s41467-022-33166-3>
- Menviel, L., Spence, P., & England, M. H. (2015). Contribution of enhanced Antarctic Bottom Water formation to Antarctic warm events and millennial-scale atmospheric CO<sub>2</sub> increase. *Earth and Planetary Science Letters*, 413, 37–50. <https://doi.org/10.1016/j.epsl.2014.12.050>
- Menviel, L., Timmermann, A., Mouchet, A., & Timm, O. (2008). Meridional reorganizations of marine and terrestrial productivity during Heinrich events. *Paleoceanography*, 23(1), PA1203. <https://doi.org/10.1029/2007PA001445>
- Menviel, L., Yu, J., Joos, F., Mouchet, A., Meissner, K. J., & England, M. H. (2017). Poorly ventilated deep ocean at the Last Glacial Maximum inferred from carbon isotopes: A data-model comparison study. *Paleoceanography*, 32(1), 2–17. <https://doi.org/10.1002/2016PA003024>
- Muglia, J., & Schmittner, A. (2015). Glacial Atlantic overturning increased by wind stress in climate models. *Geophysical Research Letters*, 42(22), 9862–9868. <https://doi.org/10.1002/2015GL064583>
- Muglia, J., Skinner, L. C., & Schmittner, A. (2018). Weak overturning circulation and high Southern Ocean nutrient utilization maximized glacial ocean carbon. *Earth and Planetary Science Letters*, 496, 47–56. <https://doi.org/10.1016/j.epsl.2018.05.038>
- Muglia, J., Somes, C. J., Nickelsen, L., & Schmittner, A. (2017). Combined effects of atmospheric and seafloor iron fluxes to the Glacial Ocean. *Paleoceanography*, 32(11), 1204–1218. <https://doi.org/10.1002/2016PA003077>

- Oppo, D. W., Curry, W. B., & McManus, J. F. (2015). What do benthic  $\delta^{13}\text{C}$  and  $\delta^{18}\text{O}$  data tell us about Atlantic circulation during Heinrich Stadial 1? *Paleoceanography*, 30(4), 353–368. <https://doi.org/10.1002/2014PA002667>
- Pöppelmeier, F., Jeltsch-Thömmes, A., Lippold, J., Joos, F., & Stocker, T. F. (2023). Multi-proxy constraints on Atlantic circulation dynamics since the last ice age. *Nature Geoscience*, 16(4), 349–356. <https://doi.org/10.1038/s41561-023-01140-3>
- Rahmstorf, S. (2024). Is the Atlantic overturning circulation approaching a tipping point? *Oceanography*, 37(3), 16–29. <https://doi.org/10.5670/oceanog.2024.501>
- Repschläger, J., Zhao, N., Rand, D., Lisiecki, L., Muglia, J., Mulitza, S., et al. (2021). Active North Atlantic deepwater formation during Heinrich Stadial 1. *Quaternary Science Reviews*, 270, 107145. <https://doi.org/10.1016/j.quascirev.2021.107145>
- Russell, J. L., & Dickson, A. G. (2003). Variability in oxygen and nutrients in South Pacific Antarctic Intermediate Water. *Global Biogeochemical Cycles*, 17(2), 1033. <https://doi.org/10.1029/2000GB001317>
- Schmittner, A. (2005). Decline of the marine ecosystem caused by a reduction in the Atlantic overturning circulation. *Nature*, 434(7033), 628–633. <https://doi.org/10.1038/nature03476>
- Schmittner, A. (2024a). OSU-UVic Climate Model Version 2.9.10 with Diagnostic Tracers for Carbon and Carbon-13 Decomposition [Software]. Oregon State University. Retrieved from <https://github.com/OSU-CEOAS-Schmittner/UVic2.9>
- Schmittner, A. (2024b). OSU-UVic hosing run with LGM initial conditions (LGM Full) [Dataset]. Zenodo. <https://doi.org/10.5281/zenodo.14231978>
- Schmittner, A. (2025a). Impact of circulation changes on carbon-13 components in the ocean. *Global Biogeochemical Cycles*, 39, e2025GB008527. <https://doi.org/10.1029/2025GB008527>
- Schmittner, A. (2025b). OSU-UVic hosing run with preindustrial initial conditions (PI Full) [Dataset]. Zenodo. <https://doi.org/10.5281/zenodo.14774855>
- Schmittner, A., Brook, E. J., & Ahn, J. (2007). Impact of the ocean's overturning circulation on atmospheric CO<sub>2</sub>. In A. Schmittner, J. C. H. Chiang, & S. R. Hemming (Eds.), *Ocean circulation: Mechanisms and impacts* (Vol. 173, pp. 209–246). American Geophysical Union (AGU). Retrieved from <https://ir.library.oregonstate.edu/concern/defaults/z603qz979>
- Schmittner, A., & Fillman, N. J. (2024). Carbon and carbon-13 in the preindustrial and glacial ocean. *PLOS Climate*, 3(7), e0000434. <https://doi.org/10.1371/journal.pclm.0000434>
- Schmittner, A., & Galbraith, E. D. (2008). Glacial greenhouse-gas fluctuations controlled by ocean circulation changes. *Nature*, 456(7220), 373–376. <https://doi.org/10.1038/nature07531>
- Schmittner, A., Gruber, N., Mix, A. C., Key, R. M., Tagliabue, A., & Westberry, T. K. (2013). Biology and air-sea gas exchange controls on the distribution of carbon isotope ratios ( $\delta^{13}\text{C}$ ) in the ocean. *Biogeosciences*, 10(9), 5793–5816. <https://doi.org/10.5194/bg-10-5793-2013>
- Schmittner, A., & Lund, D. C. (2015). Early deglacial Atlantic overturning decline and its role in atmospheric CO<sub>2</sub> rise inferred from carbon isotopes ( $\delta^{13}\text{C}$ ). *Climate of the Past*, 11(2), 135–152. <https://doi.org/10.5194/cp-11-135-2015>
- Somes, C. J., & Oschlies, A. (2015). On the influence of “non-Redfield” dissolved organic nutrient dynamics on the spatial distribution of N<sub>2</sub> fixation and the size of the marine fixed nitrogen inventory. *Global Biogeochemical Cycles*, 29(7), 973–993. <https://doi.org/10.1002/2014GB005050>
- Tierney, J. E., Zhu, J., King, J., Malevich, S. B., Hakim, G. J., & Poulsen, C. J. (2020). Glacial cooling and climate sensitivity revisited. *Nature*, 584(7822), 569–573. <https://doi.org/10.1038/s41586-020-2617-x>
- Weaver, A. J., Eby, M., Wiebe, E. C., Bitz, C. M., Duffy, P. B., Ewen, T. L., et al. (2001). The UVic Earth system climate model: Model description, climatology, and applications to past, present and future climates. *Atmosphere-Ocean*, 39(4), 361–428. <https://doi.org/10.1080/07055900.2001.9649686>
- Weijer, W., Cheng, W., Garuba, O. A., Hu, A., & Nadiga, B. T. (2020). CMIP6 models predict significant 21st century decline of the Atlantic meridional overturning circulation. *Geophysical Research Letters*, 47(12), e2019GL086075. <https://doi.org/10.1029/2019GL086075>
- Wendt, K. A., Nehrbass-Ahles, C., Niezgoda, K., Noone, D., Kalk, M., Menviel, L., et al. (2024). Southern Ocean drives multidecadal atmospheric CO<sub>2</sub> rise during Heinrich Stadials. *Proceedings of the National Academy of Sciences*, 121(21), e2319652121. <https://doi.org/10.1073/pnas.2319652121>
- Zeebe, R. E., & Wolf-Gladrow, D. (2001). *CO<sub>2</sub> in seawater: Equilibrium, kinetics, isotopes* (No. 65). Elsevier. (Google-Books-ID: g3j3Zn4kEscC).